[redacted]

FILE # [illegible]

10

Final Report

STAT **AUTOMATIC FOCUSING TECHNIQUES**

[redacted]

Declass Review by
NIMA/DOD

[redacted]

AT

Copies 2 through 9
received 19 Sep 66

August 1966

Final Report

AUTOMATIC FOCUSING TECHNIQUES

STAT

By

[redacted]

STAT

[redacted]

Copy No. 2

ABSTRACT

Various techniques for automatic focus detection and correction are reviewed for application to a rear-projection viewer operating in a scanning mode. The technique selected for detailed theoretical and experimental study automatically detects the sharpness of focus of an externally generated pattern that is projected onto the film and reimaged externally by the same optical projection system whose focus is being controlled.

Experimental results are described in the first section, which demonstrate the soundness of the technique over a practical range of parameter values. A theoretical analysis in Sec. II gives a clear basis for understanding the form of the experimental curves in Sec. I.

CONTENTS

ABSTRACT iii

LIST OF ILLUSTRATIONS vii

SUMMARY AND CONCLUSIONS ix

I AUTOMATIC FOCUSING SYSTEM. 1

A. Requirements. 1

B. Focus-Detection Methods 5

1. Film-Plane Position or Lens-Position Detection and Control. 5
2. Image Sharpness Detection. 8

C. Externally Generated Image for Focus Detection. . . 9

1. Methods of Detecting Sharp Focus of Reflected Image of Mask. 11
2. Method for Sensing Direction of Defocus. . . . 14

D. Experimental Results. 15

E. Analysis of System Accuracy 30

F. Experimental Focus-Detection System 38

G. Conclusions 39

II THEORETICAL ANALYSIS 41

A. Single Defocus. 41

1. Basic Problems of Analysis 41
2. Geometric Form for Analysis--Disk Object . . . 45
3. Preview of Analytical Steps. 46
4. Specular Light Loss--Point Source. 47
5. Disk Object--Total Light Return. 55
6. Defining the Critical Values Δp_c^+ and Δq_{Mc}^-. . . 56
7. Defining the Critical Values Δp_c^- and Δq_{Mc}^+. . . 61
8. Intercepted Light Over Range $0 \leq \Delta p \leq \Delta p_c^+$ 63
9. Intercepted Light Over Range $0 \leq \Delta p \leq \Delta p_c^-$ 65

B. Double Defocus. 67

APPENDIX A--DERIVATION OF FOCUS ERROR EQUATION. A-1

APPENDIX B--CONVOLUTION OF CIRCLES OF DIFFERENT DIAMETERS . . B-1

APPENDIX C--PROOF OF NO TRUNCATION LOSS IN RANGE
$0 \leq \Delta p \leq \Delta p_t$ C-1

APPENDIX D--PROOF OF NO TRUNCATION LOSS IN THE RANGE
$0 \leq \Delta p \leq \Delta p_c$ D-1

ILLUSTRATIONS

Fig. I-1	Film-Plane Detection.	6
Fig. I-2	Basic Layout for Focus Detection with Externally Generated Image.	10
Fig. I-3	Method for Detecting Defocused Light from Front of Mask.	12
Fig. I-4	Use of Beamsplitter and Negative Mask to Detect Defocus.	13
Fig. I-5	Laboratory Setup Used for Experimental Focus-Detection Studies	15
Fig. I-6	Basic Response Curve for m = 3.	17
Fig. I-7	Returned-Light Path with Mask Off Axis. . . .	20
Fig. I-8	Response with Mask Off Axis	21
Fig. I-9	Returned-Light Paths for Angular Film Displacement.	22
Fig. I-10	Effect of Angular Displacement of Film Surface	23
Fig. I-11	Restoration by Off-Axis Mask Placement of Light Lost Because of Angular Film Displacement.	24
Fig. I-12	Compensation for Angular Film Displacement by Off-Axis Mask Placement.	25
Fig. I-13	Return from Film Compared to Specular Return from Plane Mirror	26
Fig. I-14	Basic Response Curve for m = 1.0.	27
Fig. I-15	Basic Response Curve for m = 10	28
Fig. I-16	Multiple Mask Pattern	29
Fig. I-17	Effect of Multiple Mask	29
Fig. I-18	Dimensions Used in Analysis of System Accuracy.	32
Fig. I-19	Effect of Change in Mask Position with Respect to Screen Position.	33
Fig. I-20	Effect of Difference in Focal Length for Visual and Focus-Detection Wavelengths. . . .	34
Fig. I-21	Effect of Compensating for Focal-Length Difference with a Fixed Mask-Position Correction.	35

Fig. I-22	Experimental System for Simulating a Rear-Projection Viewer.	38
Fig. II-1	Incident Cone I and Reflected Cone R from Mirror.	42
Fig. II-2	Change in Magnification with Mirror Movement Δq_M.	42
Fig. II-3	Detection of Intercepted Light in Object Plane	45
Fig. II-4	Form of Total Returned Light L_T and Intercepted Light L_I as Functions of Mirror Position Δq_M.	46
Fig. II-5	Returned-Light Disk in Lens Plane	48
Fig. II-6	Relationship of Light Disk and Lens Disk with Mirror Outside Image Plane	49
Fig. II-7	Corresponding Values of Δq_M^- and Δq_M^+ Leading to Identical Shapes of A(r) Curves in Fig. II-5(b).	51
Fig. II-8	Range of r Over Which Common Area A has Maximum Value	52
Fig. II-9	Fraction of Returned Light for a Point Source on Axis as a Function of Δq_M^+	53
Fig. II-10	Fraction of Returned Light Over Range $q/2 \leq \lvert\Delta q_M^-\rvert \leq q$	54
Fig. II-11	Point Source r Reimaging at r'' Causing a Light Disk of Diameter W' in Object Plane with Center at Distance S' from Axis.	57
Fig. II-12	Relationship of Object Disk and Returned-Light Disk Truncated by Lens.	58
Fig. II-13	Geometrical Configuration at Critical Values Δp_c^+ and Δp_c^-	60
Fig. II-14	Use of Diffuser Instead of Mirror in Image Plane	67
Fig. B-1	Arrangement for Computing Common Area Between Two Unequal Overlapping Disks	B-3
Fig. B-2	Computation of Overlap Area for Small Values of Separation	B-5
Fig. B-3	Computer-Generated Curves of Common Area as a Function of Separation S Over the Range $R - r \leq S \leq R + r$ for Different Radius Ratios. .	B-7
Fig. D-1	Geometric Configuration for $\Delta p = \Delta p_c^-$.	D-3

SUMMARY AND CONCLUSIONS

Several techniques for automatic focus detection were examined in the context of a general set of requirements for an automatic focusing device. At an early stage in the project it was determined that the most probable application for automatic focusing would be to the scanning mode of operation of a rear-projection viewer.

On the basis of this application, the possible focus-detection techniques were reviewed, and the technique of using an externally generated image was selected for detailed study.

Section I of the report reviews this selection of a focus-detection technique and presents the results of the analytical and experimental work on automatic focus detection. Section II of the report contains the detailed theoretical analysis of the basic focus-detection technique. The four appendices contain derivations of equations used in the analysis.

The two major conclusions of this report are as follows.

(1) A focus-detection technique has been developed that detects the sharpness of an image formed by the optical system whose focus is being controlled. This technique is particularly suited to application for the automatic focusing of a rear-projection viewer during the scanning mode of operation.

(2) The theoretical and experimental results justify the engineering design and installation of a prototype focus-detection system in an existing rear-projection viewer. This will permit actual quantitative performance measurements to be made and operational experience gained to confirm the advantages of automatic focus detection.

A parallel research program should be continued on extensions of the basic focusing techniques and on modifications for other applications.

I AUTOMATIC FOCUSING SYSTEM

A. Requirements

A detailed and specific set of requirements for an automatic focusing system will depend upon the specific type of equipment in which an automatic focusing technique would be employed and upon the capabilities of the given technique chosen for the selected application. The following objectives for an automatic focusing system were provided by the sponsor prior to the beginning of this project as an informal guide to what is desired in an automatic focusing system for a variety of possible applications.

(1) Resolution: Resolution sensitivity at the output presentation (the point where the original is examined by the eye) of greater than 10 line pairs per millimeter.

(2) System Response: The system must sense, respond to, and correct--by changing the projection-lens position--variations in the object plane position of up to ±1/4 inch. This must be accomplished at a rate faster than the response time of the eye.

(3) Energy Required: The illumination required from the projected image should be a minimum. The maximum illumination reduction should be 10 percent. This light-subtraction technique (beam-splitter in projection path) is preferable to sensors in the image plane.

(4) The system should be completely automatic, not requiring periodic calibration. The system should average any curvature in the object plane; however, it should consider only that portion of the image which is actually being projected.

(5) Magnification Ranges: The equipment that this device would be used on has a range of magnification from one to fifty diameters.

(6) Equipment: This system is to be used on rear-projection viewers, photographic enlargers, direct-viewing equipment, etc.

The following paragraphs interpret the preceding list of objectives and relate them in a qualitative manner to the scope and results of our research.

At the beginning of the project work a review of the scope of the research with the project monitor determined that the most likely application of an automatic focusing system would be on a rear-projection film viewer of the type used to scan large quantities of aerial film. Therefore, the study of those automatic focusing techniques that would have application for rear-projection film viewers would be emphasized in the basic research work. The following comments are numbered to correspond to the objectives listed above.

(1) and (4): The resolution of the output presentation will be limited by the capability of the given optical system and film combination in a particular type of equipment. How close to this limiting performance the equipment will actually operate is dependent upon many peripheral items of which correct adjustment of focus is a primary operational limitation. In the static situation with the film held flat and perpendicular to the optical axis, the correct adjustment of focus may be accomplished satisfactorily by careful manual procedures. However, under the conditions specified for the scanning mode in a rear-projection film viewer, both the position of the film plane and its "flatness" are continually varying at a rate that precludes manual focusing.

The ultimate in performance of any automatic focusing system will be basically limited both by the curvature of the film and by any angular deviation of the film from the normal film plane. Because of these

uneven displacements of the film from the film plane, it is likely that only a portion of the overall film image can be critically focused at any one instant.

A focus-detection system that could examine the entire image area and select an average plane of focus to maximize the area of the negative in or near critical focus is not practical with any of the focus-detection ideas developed under this project.[1] The best that can be accomplished is to critically focus the center portion of the image area--i.e., that part centered on the optical axis of the projection system.

It is felt that this is a satisfactory compromise and that this method may actually prove to be operationally more desirable than an averaging approach. When the operator stops the scanning mode and desires to examine a given area in more detail (and/or at a higher magnification), the centering of the desired area will thus automatically ensure critical focus for the given section being examined.

(2): For the typical lens sizes employed in a rear-projection film viewer employing film up to 9 inches wide, the direction of the variation of the film plane (to $\pm \frac{1}{4}$ inch) can be sensed for magnifications up to a value of 15 to 20. At greater magnifications the allowable range over which the direction of defocus can be detected becomes restricted. Section II develops the formulas that relate the range over which the direction of defocus can be sensed to the other parameters of the system.

The speed with which the system can sense defocus is rapid--measured in milliseconds. The correction of focus by movement of the lens will be slower and will be the primary limitation of the response time of the system. The design of the servo system to control the lens was not studied on this project. However, consideration of the problem in relation to the sizes of lenses required and the distances over which they must move suggests that a system response measured in tenths of a second

---

[1] See discussion in Sec. I-B.

could be realistically expected. Considering the light mass of the film and the viscous damping of the air, the speed with which the film will move from the film-plane position during scanning may be slow enough that a servo response of 1/10 second will permit the focus system to follow the film movement. Measurement of the actual rates of displacement from the film plane on a film viewer during the scanning mode should be made and the system response specifications related to these figures.

It should be noted that the tension between the two rolls driving the film will have a direct effect on both the magnitude of the film displacement and the frequency with which it varies. As the tension is increased, this will reduce the magnitude of the film displacement from the film plane and will increase the frequency at which the film will tend to vibrate or move in and out of the film plane. Reducing the tension will tend to reduce the frequency with which the film moves but will most likely permit it to make a wider excursion. A study of this relationship should be made to determine the best tension and drive characteristics for the film transport in relation to an automatic focusing system, in terms of the range over which the focus detection system can operate and the speed with which it can correct focus by moving the lens. This will permit the optimum arrangement of these parameters to achieve the best overall system performance.

(3): The technique of imaging an external pattern onto the film for the purpose of focus detection will require no energy from the film image. By using a projected image of the external pattern in a wavelength band at the edge of the visual spectrum and with the proper design of the additional optical components required to place this image in the optical path, none or at most a very few percent of the illumination from the visual film image will be attenuated.

(5): A magnification range of 1 to 50 was specified in this preliminary requirement but later modified in discussions with the project monitor to a range of 3 to 70. As indicated above, at the present state of development of the focus-detection system the requirements of ±1/4-inch film deviation can be handled at low magnification ranges extending

up to approximately the range of 15 to 20. Beyond that point the focus-detection system continues to operate in the region near correct focus, but the range of defocus over which the system can sense the correct direction required to correct focus gradually diminishes. A study of the magnifications at which the scanning mode of operation is likely to be operated may show that it is not necessary to maintain the ±1/4-inch requirement for the higher magnifications. Since the highest magnifications will undoubtedly be used for the static examination of a small area of the film, the system could be manually returned to near focus in the event that a rapid transient produced an error too large for the system to follow. The automatic system would take over and maintain focus for the slow variations that might occur during the static examination of a given area.

(6): The focus-detection technique developed is applicable to all the various types of equipment mentioned, although emphasis was placed on use during the scanning mode of the rear-projection film viewer. The requirements for this application are in general the most difficult to meet.

B. Focus-Detection Methods

Focus-detection techniques can be divided into two basic categories:

1. Film-Plane Position or Lens-Position Detection and Control

The techniques grouped in this class do not examine the projected image for sharpness of focus. Instead, a measurement of film or lens position is made for a given set of conditions with the system set for correct focus. The system then monitors and controls the film or lens position to maintain this given film-lens relationship. If all other parameters affecting focus remain unchanged, then the correct positioning of the film plane or lens position will result in correct focus.

Systems employing such techniques are widely used in professional film-enlarger equipment and in several deluxe film projectors for 35 mm color slides. The following paragraphs illustrate how these

two techniques can be implemented. The descriptions are not intended to detail any specific implementation.

In the enlarger application, the lens-to-film spacing is varied by a carefully computed, precision-made mechanical cam system. This cam system varies the lens-to-film spacing as a function of the height of the enlarger head (containing lamphouse, film, and lens) above the baseboard where the image is projected onto the printing paper. When the enlarger is carefully focused manually at any given height above the baseboard, then the focus is automatically maintained over the entire range of magnifications by the mechanical cam arrangement. However, such operation is assured only for the specific lens for which the mechanical cam was designed. In addition, the placement of the paper on the baseboard and of the film in the film holder and the mechanical structure holding the enlarger head must remain in exact dimensional relationship if the cam is to correctly maintain focus throughout the operational range of the enlarger.

In the projector application a small beam of light is projected onto the center of the slide at an angle, from behind and to one side of the main projection lens (see Fig. I-1).

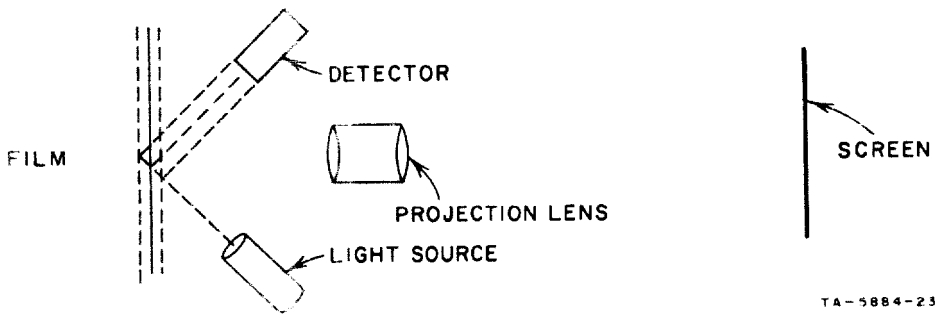

FIG. I-1 FILM-PLANE DETECTION

When the slide is in the correct position, the detector unit receives the reflected beam centered. The lens is then manually adjusted to give a sharp image at the selected screen distance. Any

change in the slide position due to differences in mounting or due to bowing from heat will be sensed by the detector as the reflected beam moves away from the center to the left or right. This signal from the detector is used to drive a servo that repositions the slide carrier to place the center of the slide back at the correct position and thus return the beam to the center of the detector.

Both of these systems perform satisfactorily for the applications described, provided they are maintained and used properly within the constraints required by their design. Neither system senses the actual sharpness (focus) of the image and consequently neither can be truly termed a focus-detection system.

The application of these techniques to this project was not considered practical, since the requirements for focus control during the scanning mode of a rear-projection film viewer preclude any control of the film-plane position. Although it would be possible to measure the film-plane position and in an open-loop fashion move the lens in a precomputed relationship to the film-plane motion to achieve focus at the projection screen, such a system would require an accurate measurement of the film-plane position over the ±1/4 inch as well as a complex functional relationship to transform this measurement into the correct lens position to achieve focus as the film varies. While this might be possible for a given focal-length it would become very complex with variable focal-length lenses. Changes in lens focal lengths are required to achieve changes in magnification in rear-projection viewers where the film-to-screen distance remains constant. This is in contrast to the enlarger application where changes in magnification are achieved with a given lens by permitting the film-to-image distance to vary.

Therefore, it is concluded that the approach offered by either of these techniques would be both difficult and subject to inaccuracies for application to rear-projection viewers.

2. Image Sharpness Detection

The second category of automatic focusing techniques includes those that detect a sharp image in the desired image plane or its optical equivalent. The detector output can then be used in a closed-loop control system to maintain the desired critical focus by adjusting any one of four primary parameters--film-plane position, image-screen position, lens position, or lens focal length.

The source of the image used by the detector to detect sharp focus can be from one of three basic sources.

a. The Image Recorded on the Film

The projection of optical images onto a nonlinear photocell to detect their sharpness is a basic technique developed in this laboratory and previously described.* The main limitation of this technique as applied to the present problem is that the film to be viewed or scanned may contain large sections of photographs of water or uniform cloud areas with little or no sharp detail in the film image. The focus-detection system would see no sharp image boundaries when such sections of the film passed the viewer and thus would not maintain sharp focus. Therefore, small but significant pinpoint areas in the field of view could go unnoticed because of the overall defocused position of the image. Because of this serious limitation from an operational point of view, this technique was considered marginal for application to the scanning mode of a rear-projection film viewer.

b. Grain in the Film Image

The tight, sharp grain pattern that exists in modern films makes an ideal pattern for detection by the nonlinear-photocell

---

*J. C. Bliss and H. D. Crane, Relative Motion and Nonlinear Photocells in Optical Image Processing, in Optical and Electro-Optical Information Processing (M.I.T. Press, Cambridge, Massachusetts, 1965).

J. C. Bliss and H. D. Crane, "Optical Detector for Objects Within an Adjustable Range," J. Opt. Soc. Am., Vol. 54, No. 10, pp. 1261-1266 (1964).

technique. However, it requires magnification by 100 to 200 diameters before projection onto the nonlinear photocell. If a rear-screen projection system were to operate at a constant magnification ratio, the additional magnification could be optically inserted to enlarge the grain pattern on a nonlinear photocell and make this a possible approach. However, with the wide range of magnifications that are desirable, the use of the film grain as a basic focusing image becomes difficult. The secondary optical system required would have to have a magnification that would vary inversely with the main optical system and would have to maintain the same relative focus distances. Such a subsystem would be in series with the focus-detection element, and any variations or shifts in its focus with magnification change would create errors in the overall focus-detection system. While these could be minimized by careful design and engineering, this system would be more difficult to implement than the following method for obtaining an image source for automatic focus detection.

c. Externally Generated Image

This technique appears to be the most versatile and offers the best combination of advantages for application to automatic focusing systems and in particular to the rear-projection systems during scanning modes. The majority of the project effort was spent in examining this technique both experimentally and analytically. The remainder of the report will therefore deal with a description and analysis of this method of automatic focus detection.

C. Externally Generated Image for Focus Detection

Figure I-2 indicates the basic technique of how an exterior image is projected onto the film and used for focus detection.

A dichroic mirror that reflects infrared but is transparent to visual light is inserted at a 45° angle just beyond the last element of the projection lens system. An illuminated mask is placed on the new optical axis defined by the 45° mirror and at the same distance from the center of the mirror as the viewing screen. This results in the

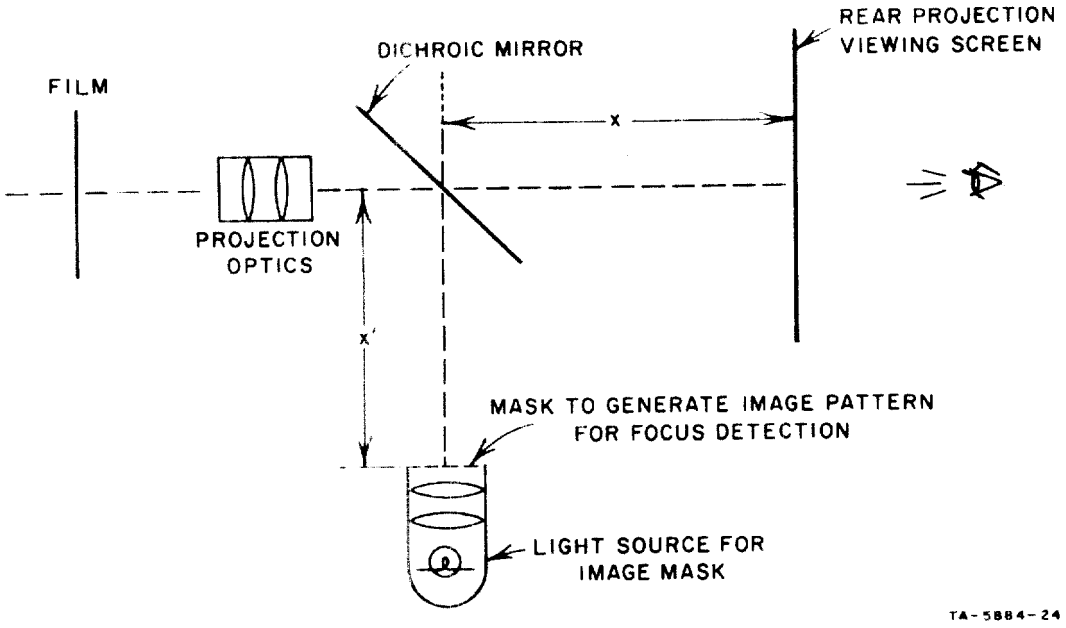

FIG. I-2 BASIC LAYOUT FOR FOCUS DETECTION WITH EXTERNALLY GENERATED IMAGE

lens system imaging the illuminated pattern of the mask onto the film in exact focus when the optical system is adjusted to project the film image into exact focus on the screen.* The surface of the film spectrally reflects several percent of the infrared light of the projected pattern back through the lens and the dichroic mirror, where it is refocused in the plane of the illuminated mask. The use of an infrared-reflecting filter between the film and the projection light source (not shown in Fig. I-2) prevents infrared light from the projection light source from interfering with the focus-detection system. Because of the geometry of the system (see Fig. I-2), where x is made equal to x′, the reflected image of the mask at the location of the mask is only in focus when the film image is in focus on the screen. For any other film position, both the reflected image of the mask and the film image at the screen are out of focus.

*A discussion of the effects resulting from the infrared and visual focal lengths of the projection optics having slight differences is given in Sec. I-E.

1. Methods of Detecting Sharp Focus of Reflected Image of Mask

When the reflected image of the mask is in exact focus, all the light originating from the mask aperture returns through the aperture, and no illumination falls on the surface of the mask facing the lens. When the film plane is not in exact focus, the return image is also out of focus and light now falls on this surface, surrounding the aperture. Three methods have been considered to detect the defocused light on the front of the mask.

Use of Photoconductor Surface on Mask--If the front surface of the mask is coated with photoconductive material and electrodes are placed to measure the change in conductivity resulting from the light of the defocused image, the change in conductivity between the electrodes will give an indication of the amount of light impinging on the front surface of the mask. Sharp focus will be indicated when the minimum amount of light falls on the mask, and this will be indicated by the minimum conductivity of the photoconductive surface. This method is simple to implement optically but is complicated by the necessity of fabricating a specialized mask photocell. Difficulties in obtaining specialized photocell surfaces on various experimental masks made this an unattractive approach for the experimental phase of the project. However, were an application to be employed with a large number of identical units, serious consideration of this technique would be warranted.

Detection of Light Reflected from Front Surface of Mask--The placement of small-angled mirror surfaces or the use of a smooth white diffusely reflecting surface permits a portion of the light falling on the front of the mask to be collected by a photodetector placed off to the side of the optical path. Figure I-3 indicates how this approach would be implemented with the use of small mirrored surfaces. The use of a diffusing surface is simpler and is the technique that was employed during the laboratory experimentation phase of this project. The diffusing surface is an inefficient reflector of light, and the photodetector receives only a small portion of the light falling on the front side of the mask. For this reason, a highly sensitive

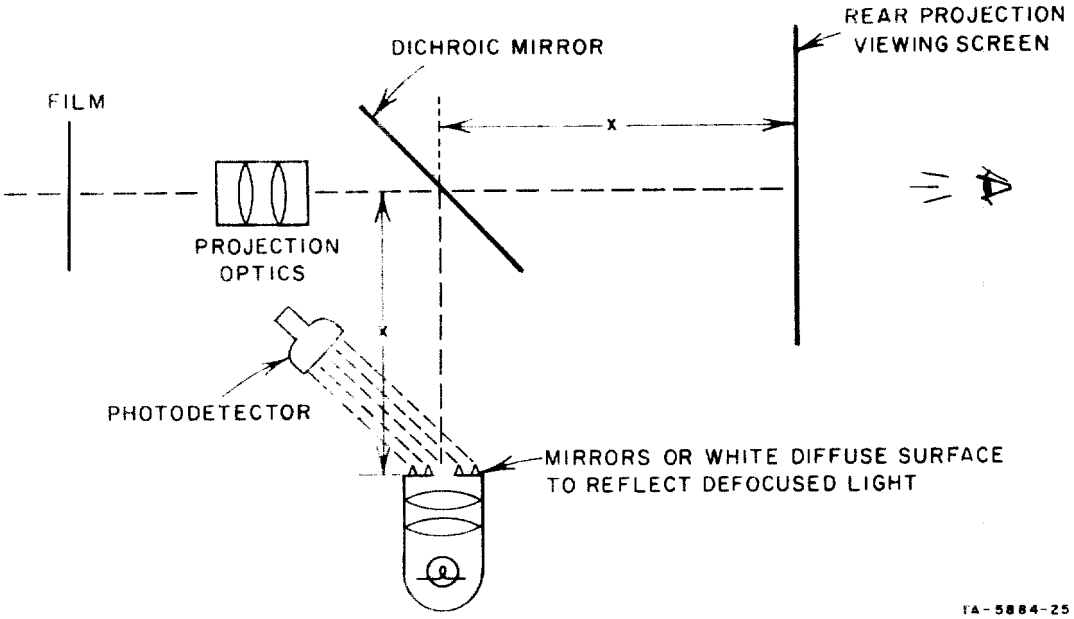

FIG. I-3 METHOD FOR DETECTING DEFOCUSED LIGHT FROM FRONT OF MASK

photomultiplier tube was employed during the experimental work. The use of the diffuse surface permitted the aperture pattern in the mask to be of any desired shape. The use of mirrored surfaces would be more difficult with the circular patterns that were employed. For vertical slits, the mirrored surfaces would be more feasible and more efficient than the diffuse surface. This approach separates the mask from the photodetector and provides the flexibility desired for experimental work.

Use of Beam Splitter and Negative Mask--As shown in Fig. I-4, a 50-percent reflection mirror is mounted at a 45° angle in front of mask 1 to reflect a portion of the reflected mask image to the location of mask 2. Mask 2 has a pattern identical to that of mask 1 but is a negative (transparent areas are opaque and opaque areas are transparent in relation to mask 1). Thus a sharp image returning toward mask 1 is reflected to mask 2 which intercepts all of the in-focus image. When defocus occurs, some light then passes through to a photodetector located behind mask 2. Any photodetector can be used, and it is relatively easy to gather all the light that passes mask 2. The introduction of the second half-transmission mirror results in a 4-to-1 light loss when

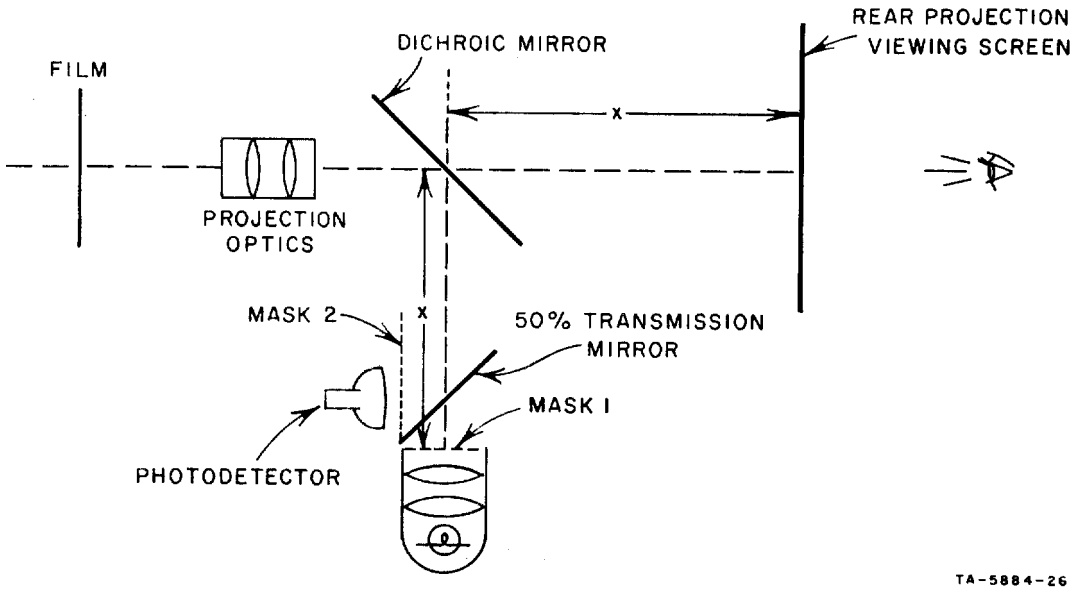

FIG. I-4 USE OF BEAMSPLITTER AND NEGATIVE MASK TO DETECT DEFOCUS

compared to the light that would fall on the face of mask 1. Any mask pattern, however, can be used and even with the 4-to-1 light loss due to the mirror, the efficiency in collecting the return light is probably better than most of the arrangements for measuring light reflected from the mask. A preliminary test setup using a positive and negative mask consisting of parallel slits and bars was used in one of the breadboard configurations (see Sec. I-F). The method was not used on the detailed experimental studies of mask characteristics, however, because of the necessity of making the inverse shape for mask 2 and the necessity of carefully aligning the two masks and the mirror for each change in the experimental configuration. This method has the advantage of offering the freedom to use any standard photodetector. In addition, no specialized mirrored surfaces are required. The light-gathering capacity is reasonably efficient and is independent of the particular mask design, though some limitations are imposed on mask design by the requirement of the negative mask. This method would warrant serious consideration for a prototype design.

2. Method for Sensing Direction of Defocus

The point of exact focus is at the point where the minimum illumination is detected by the photodetector. However, the static photocell output does not indicate whether a minimum exists or (if the output is not a minimum) in which direction the focus must be corrected to approach the minimum.

This sensing was accomplished in our mobility-aid work using the nonlinear photocell by vibrating the photocell axially at a frequency of several hundred cycles per second and over a distance of 0.010 to 0.015 inch. The output signal from the photocell for out-of-focus images is then a sine wave of the same frequency as the photocell vibration. The phase of this sine wave reverses by 180° depending on which side of the image plane the photocell is located. Because of the symmetry of small perturbations about a sharp image plane when the photocell vibration is exactly centered on the image plane, the output signal is the second harmonic of the basic photocell vibration frequency.

A variation of this technique is required in the present application. The same second harmonic and phase-reversing fundamental sine waves can be produced by small vibrations of either mask 1 or mask 2. However, this requires planar mechanical vibration of a mask. An alternate method is the introduction into the optical path of a small optical component of variable focal length. A simple method has been devised to accomplish this by using a thin-film pellicle mirror, vibrated by air coupling from a small loudspeaker. Laboratory experiments have shown this to be an ideal way to achieve small variations in the optical path length. The vibrating mirror adds some optical complexity, but eliminates the need for vibratory systems moving significant masses--such as the masks.

An alternate method employing a three-dimensional mask and two separate detectors was conceived. A preliminary investigation of this approach revealed that a far more detailed study would be required before a meaningful description or evaluation of this approach could be made. The use of the vibrating pellicle mirror is the preferred method at present.

D. Experimental Results

In order to experimentally measure the focus-detection system response characteristics, the laboratory test system shown in Fig. I-5 was assembled. This equipment permits the measurement of the light intercepted by the mask as a function of the film position behind the

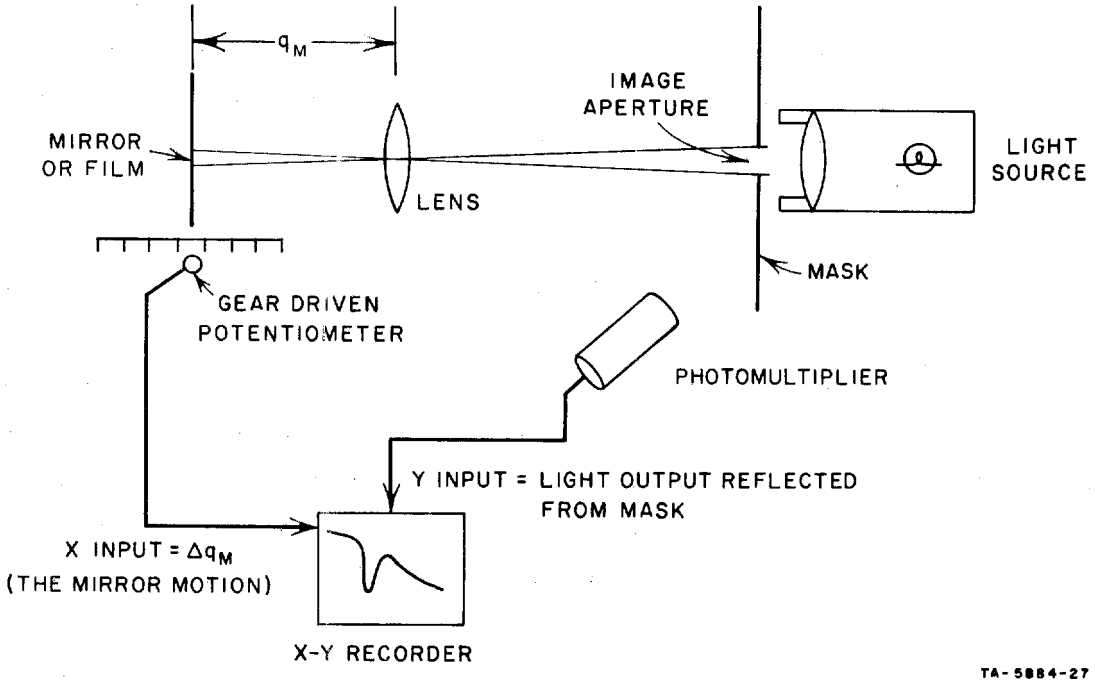

FIG. I-5 LABORATORY SETUP USED FOR EXPERIMENTAL FOCUS-DETECTION STUDIES

lens. The film for most experiments was replaced with a high-reflectance plane mirror. The mirror could also be replaced with a white diffusing surface so that the effects of diffuse reflection could be evaluated. The results of experiments confirm the theoretical analysis developed in Sec. II and the appendices. Of particular interest are the range over which "focus null response" is obtained and the effects of system misalignment.

According to the theory two system parameters are of critical importance in determining the response characteristics. These two

parameters are the magnification of the optical system, which is the ratio of mask-to-lens distance to film-to-lens distance at focus:

$$m = \frac{p}{q} \qquad \text{(I-1)}$$

where p = mask-to-lens distance and q = film-to-lens distance. The second critical parameter is the ratio of lens size to mask aperture size. This ratio is clearly defined only if the lens and the aperture have similar shapes. In order to permit comparison of experimental results with theoretical predictions, the aperture used in the following experiments is of circular shape. Thus, in the following data, the ratio of lens size to image size is

$$M_s = \frac{D}{W} \qquad \text{(I-2)}$$

where D = lens diameter and W = diameter of mask aperture. Once established by a given system, the parameters m and M_s determine the range over which focus detection can be obtained and the degree of off-axis misalignment of the mask that can be tolerated. In conjunction with the lens f-number, these parameters also determine the effect of angular misalignment of the film. The response curve for an aligned system with a magnification m = 3 and lens-to-mask ratio M_s = 9.57 is given in Fig. I-6. The amount of light intercepted by the mask as a function of film distance from the lens is indicated for both specular and diffuse reflection. Since the light reflected from the film has been determined to be mostly specular, it is this curve that is considered significant and a diffuse response is included for reference only. The principal difference between the two curves, aside from the great reduction in returned light in the diffuse case, is that the light returned for the diffuse case continues to increase as the film approaches the lens, while for the specular case, the light returned reaches a constant value. As shown in the derivation of Sec. II, the sharpness of the null is dictated by two critical values of Δq called Δq^{+}_{Mc} and Δq^{-}_{Mc}. The magnitudes of these critical values of Δq_M depend only on m and M_s and are given in Eqs. (I-3) and (I-4). These points are marked on the curve.

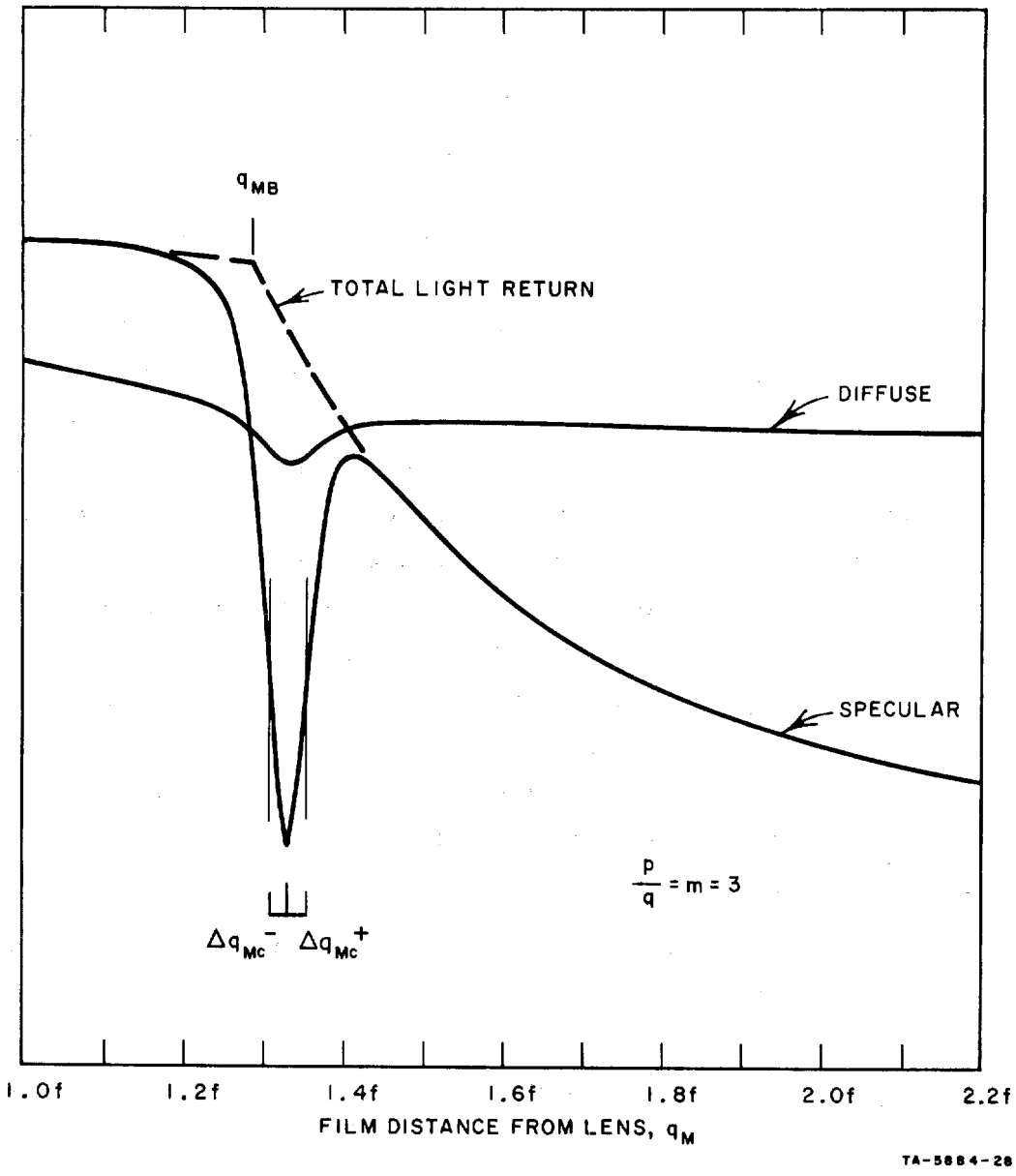

FIG. I-6 BASIC RESPONSE CURVE FOR m = 3

$$\Delta q^{+}_{Mc} = \frac{q_M}{2(mM_s - 1)} \qquad (I-3)$$

$$\Delta q^{-}_{Mc} = \frac{q_M}{2mM_s} \qquad (I-4)$$

where q_M is the in-focus distance of the film to the lens. It is clear from Fig. I-6 that the range of focus detection in the direction of film motion away from the lens is limited to approximately two increments of Δq^{+}_{Mc}. The detectable range for film motion toward the lens is approximately $2\Delta q^{-}_{Mc}$, although the limit is not clearly defined if the total light intercepted by the mask is measured. This may not be feasible in a practical system since the light return as the film approaches the lens is spread over a very large area and becomes difficult to collect. If the light-collection area at the mask is limited in extent, the left-hand portion of the curve of Fig. I-6 would not reach a nearly constant value as indicated, but would begin to decrease when the size of the returned area of light exceeded the collection area. Thus the detection range in the negative direction of film motion can be limited by practical difficulties as well as by the characteristics of the focus-detection scheme.

A reasonable estimate for the measurement range can be obtained by specifying

$$\Delta q_R = 2\left(\Delta q^{+}_{M} + \Delta q^{-}_{M}\right) \quad , \qquad (I-5)$$

which, upon substitution of Eqs. (I-3) and (I-4), becomes

$$\Delta q_R = q_M \left[\frac{2mM_s - 1}{mM_s(mM_s - 1)}\right] \qquad (I-6)$$

or, in terms of the lens focal length and magnification,

$$\Delta q_R = f\,\frac{(m + 1)(2mM_s - 1)}{m^2 M_s (mM_s - 1)} \quad . \qquad (I-7)$$

For $M_s = 9.57$ (the magnitude employed in the tested system), the detectable range is given for three magnifications in the table below.

Table I

DETECTION RANGE FOR $M_s = 9.57$

Magnification, m	Δq_R
1.0	0.44f
3.0	0.095f
10.0	0.024f

The precision of focus obtainable depends primarily on the sharpness of the null in the vicinity of focus, which in turn is a function of the quality of mask construction, stray reflections from internal lens surfaces, and aberrations of the lens at the wave length used for detection. It is estimated that a precision of $\Delta q_R/100$ should be obtainable with reasonable care in system design. It may be possible to attain precisions of $\Delta q_R/1000$ with high-quality lenses and masks.

Also plotted in Fig. I-6 is the total light returned through the lens prior to masking. The "focus null" characteristic is superimposed on this curve. As explained in Sec. II of this report, the light return as a function of film distance from the lens (q_M) is constant from $q_M = 0$ to $q_M = q_{MB}$ where q_{MB} is the point where vignetting and ray divergence cause a rapid reduction in light getting through the lens. The value of q_{MB} is given by

$$q_{MB} = q_M - \frac{q_M}{mM_s + 1} \quad . \qquad \text{(I-8)}$$

When this is compared with Eq. (I-4), it is apparent that q_{MB} always lies to the left of the focal point q_M, and is somewhere between Δq_{Mc}^- and $2\Delta q_{Mc}^-$. The interaction of the light returned and the "focus null" curves will then always result in some degree of asymmetry in the response. This asymmetry is most severe at low magnifications, but the

light level at Δq^{-}_{Mc} is always greater than at Δq^{+}_{Mc}, even though Δq^{+}_{Mc} is slightly larger than Δq^{-}_{Mc}.

It is next desired to investigate the effect of placing the mask at a distance r_p from the optical axis. As can be seen in Fig. I-7, if the mask is offset sufficiently from the optical axis, a point will be reached where no light is returned to the lens; this establishes a maximum value for r_p as given by Eq. (I-9). For the experimental system, the maximum r_p equals 1.6 lens diameters.

$$r_p\ (\max) = D/2 \left(m + \frac{1}{M_s}\right) \quad . \tag{I-9}$$

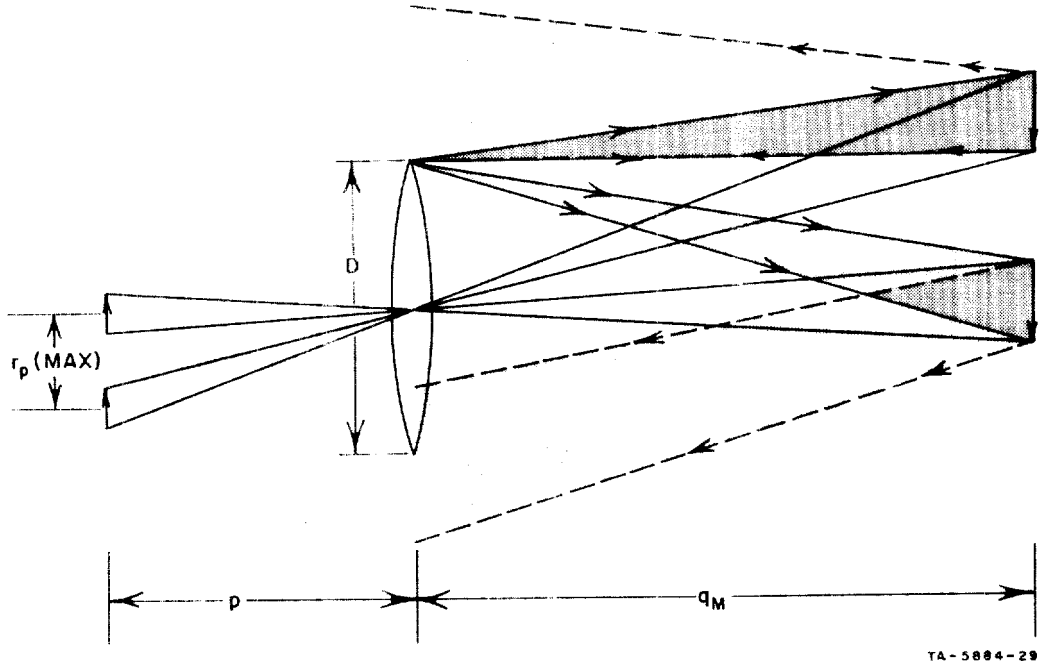

FIG. I-7 RETURNED-LIGHT PATH WITH MASK OFF AXIS

The response curve for a mask movement approximately 50 percent of this maximum is shown in Fig. I-8. Note that the sharpness of the null is reduced, but that the detection range is actually extended slightly.

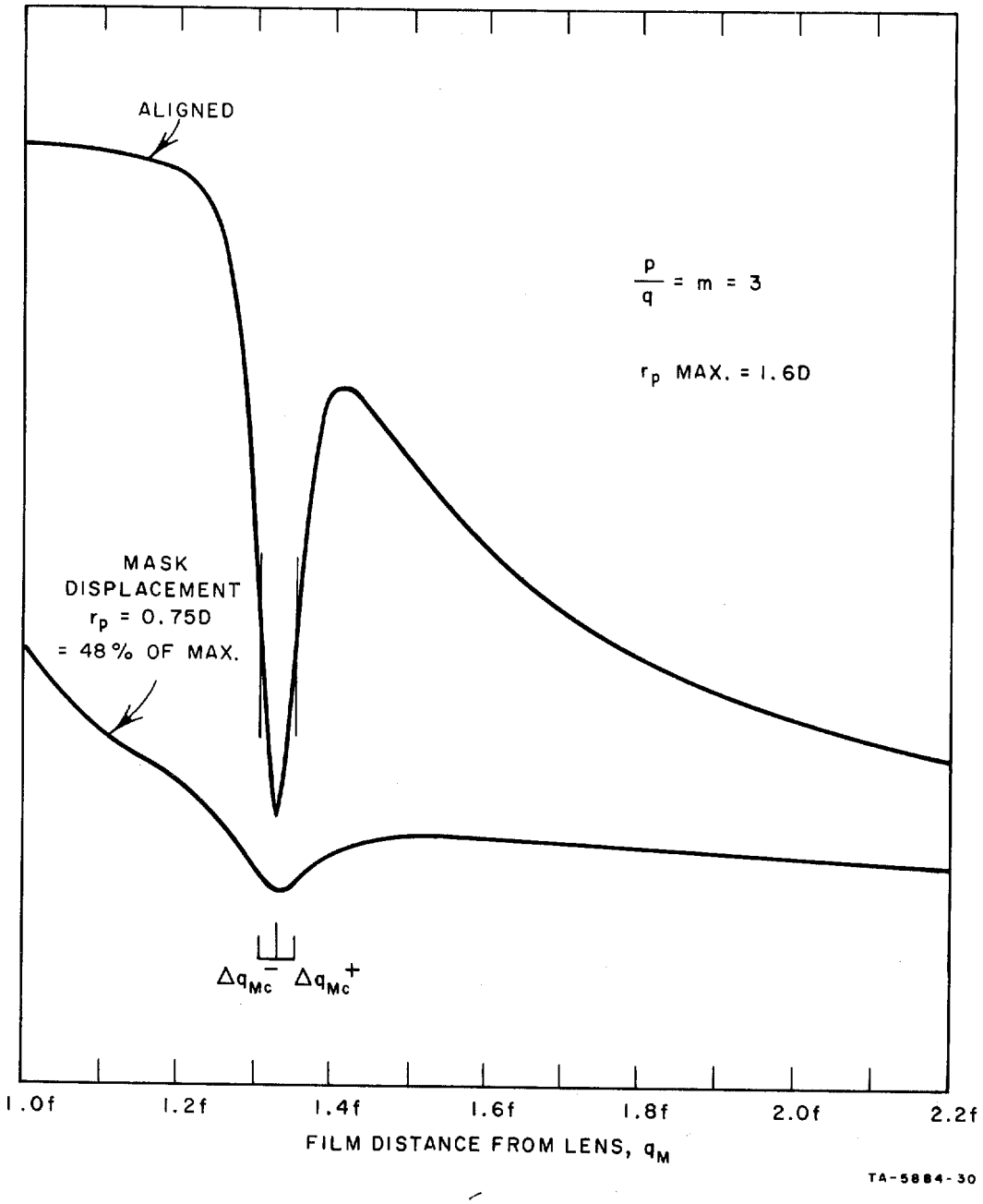

FIG. I-8 RESPONSE WITH MASK OFF AXIS

Another important possible misalignment is angular rotation of the film. This effect is shown in Fig. I-9. Again an extreme angle exists such that no light is returned to the lens. This angle is given by Eq. (I-10), where F is the lens f-number. The critical angle for the test system is equal to 8.9°.

$$\tan \theta_c = \frac{1}{2F} \left[\frac{1 + mM_s}{(m + 1) M_s} \right] . \qquad \text{(I-10)}$$

The effect of angular misalignment for various angles is given in Fig. I-10. It is apparent that satisfactory response is maintained for misalignments of as much as one-half of the critical angle. It is conceivable

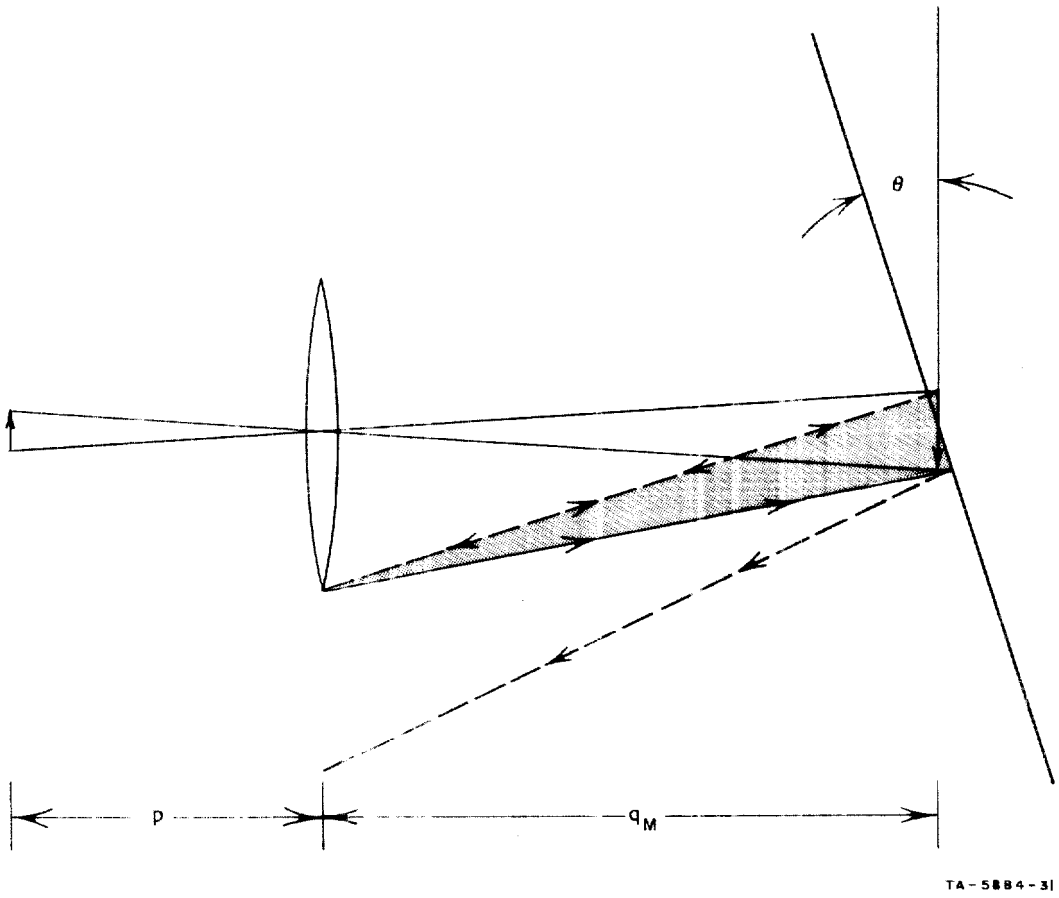

FIG. I-9 RETURNED-LIGHT PATHS FOR ANGULAR FILM DISPLACEMENT

that off-axis points can be intentionally included to help compensate for angular movement of the film. This is shown in Fig. I-11, in which for a given film rotation the off-axis mask causes the light to be returned to the lens. A test was made in which an angular deflection of

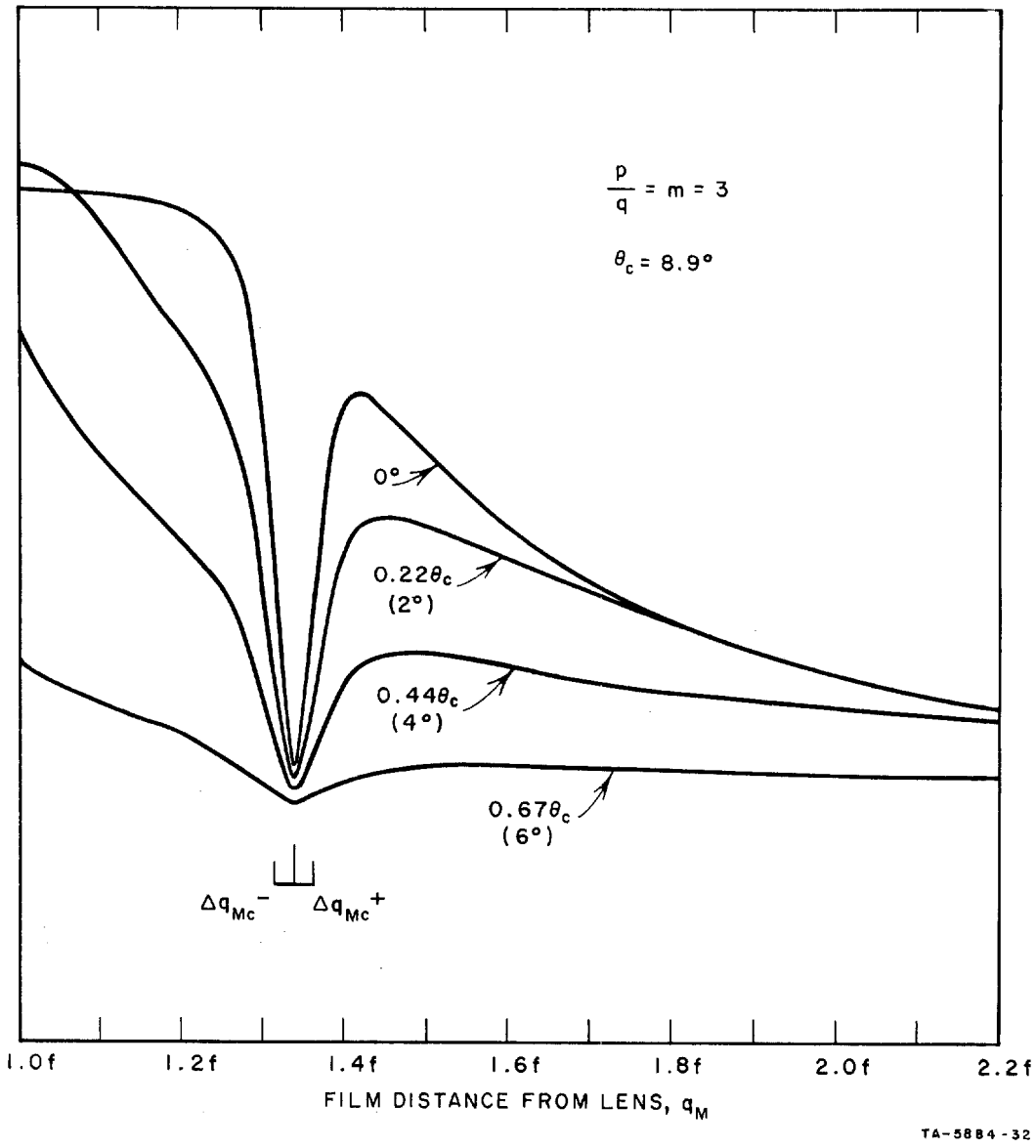

FIG. I-10 EFFECT OF ANGULAR DISPLACEMENT OF FILM SURFACE

12 percent greater than critical was produced and then compensated by moving the mask 1.4 lens diameters off-axis. The response is shown in Fig. I-12. Notice that Fig. I-12 shows the offset of the focal point as would be expected from inspection of Fig. I-11. As can be seen in Fig. I-12, this compensating effect has very nearly restored the response to that of the aligned system.

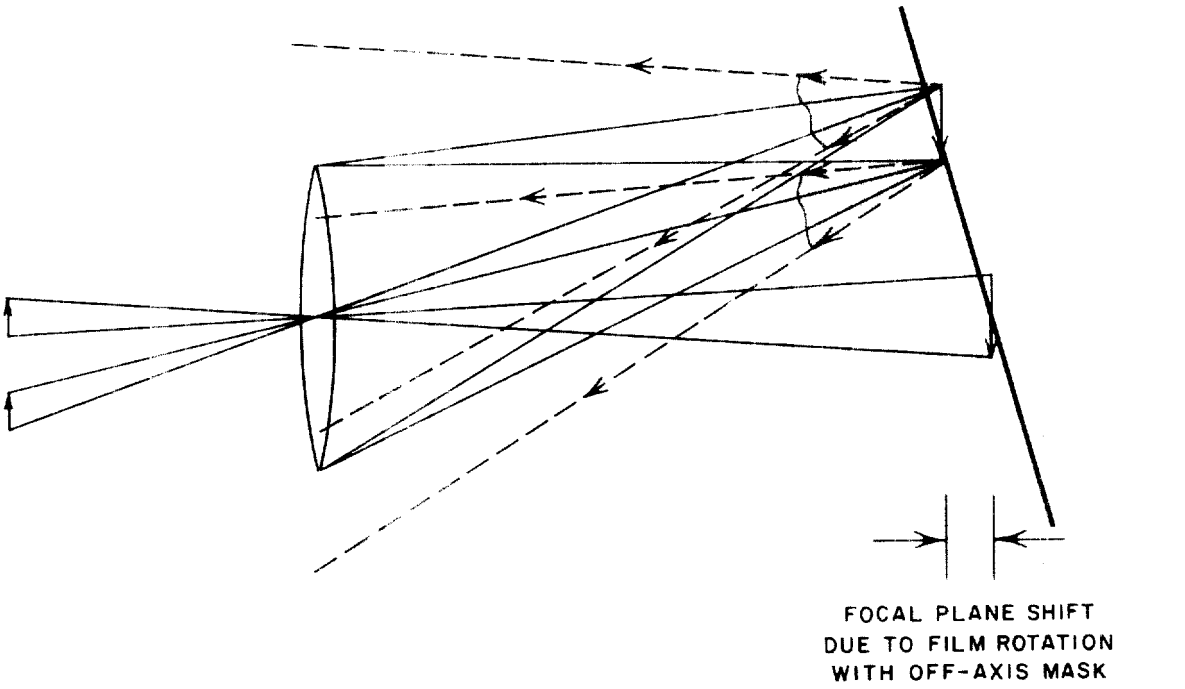

FIG. I-11 RESTORATION BY OFF-AXIS MASK PLACEMENT OF LIGHT LOST BECAUSE OF ANGULAR FILM DISPLACEMENT

In the previous curves the "film" is a highly reflective plane mirror. In order to estimate the total amount of light available from the film and to compare its response with pure spectral characteristics, the mirror was replaced with an actual piece of film. The results of this test are indicated in Fig. I-13. The lower curve indicates the film response with the source intensity unchanged from that used for the mirror curve. The source intensity was then increased so as to bring the total light return to nearly the level produced by the mirror. It is clear that there is some reduction in the depth of the null, but it is felt that most of this is due to increased background level as a result of increasing the light intensity. In a well-designed physical system, the stray light can be kept to a much lower level. Figures I-14

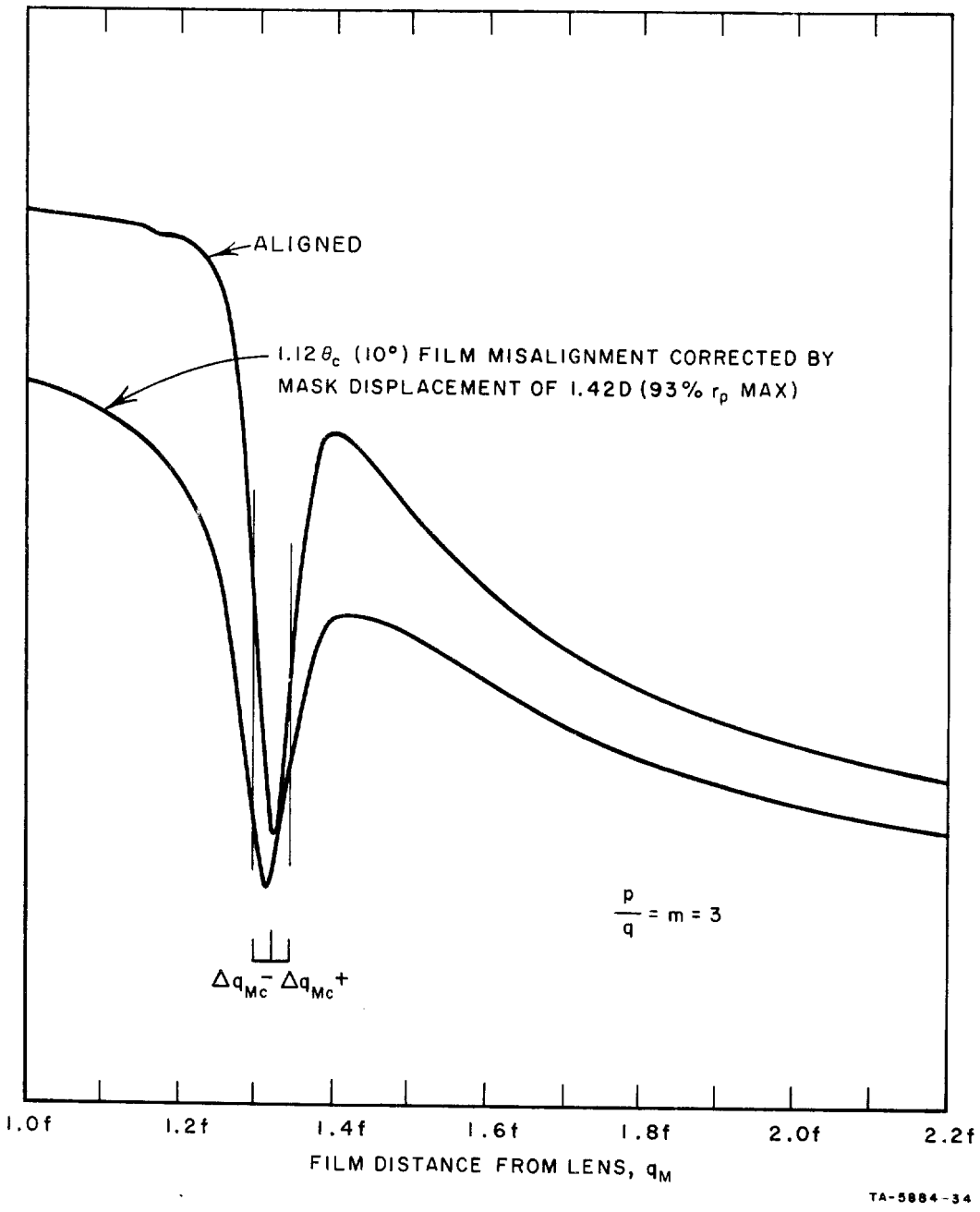

FIG. I-12 COMPENSATION FOR ANGULAR FILM DISPLACEMENT BY OFF-AXIS MASK PLACEMENT

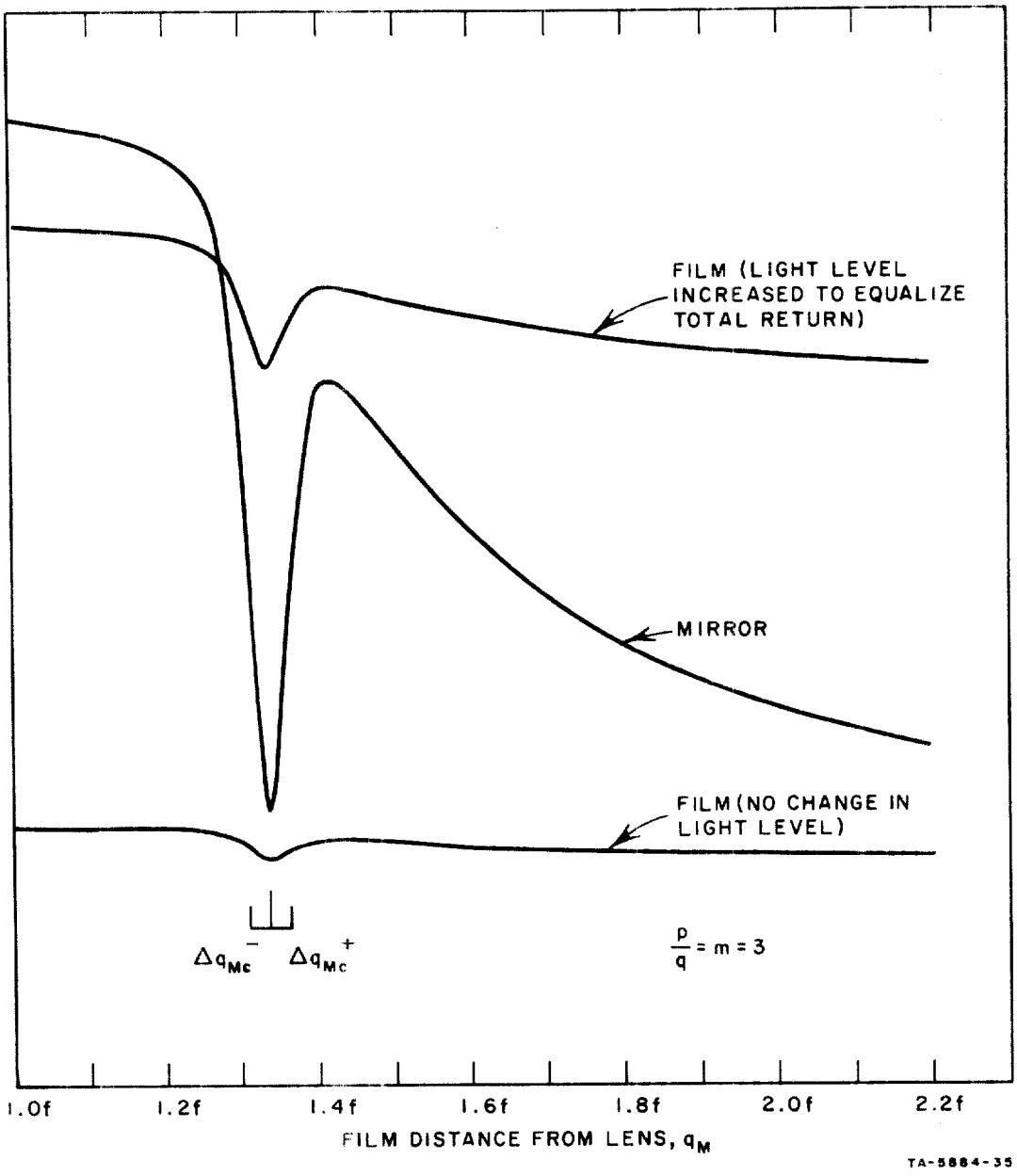

FIG. I-13 RETURN FROM FILM COMPARED TO SPECULAR RETURN FROM PLANE MIRROR

and I-15 are basic response curves made with the same lens system but at different magnifications. In Fig. I-14 m = 1.0, and in Fig. I-15 m = 10. It is clear from both of these figures that the sharp break in the returned light characteristics occurs when the film moves a distance

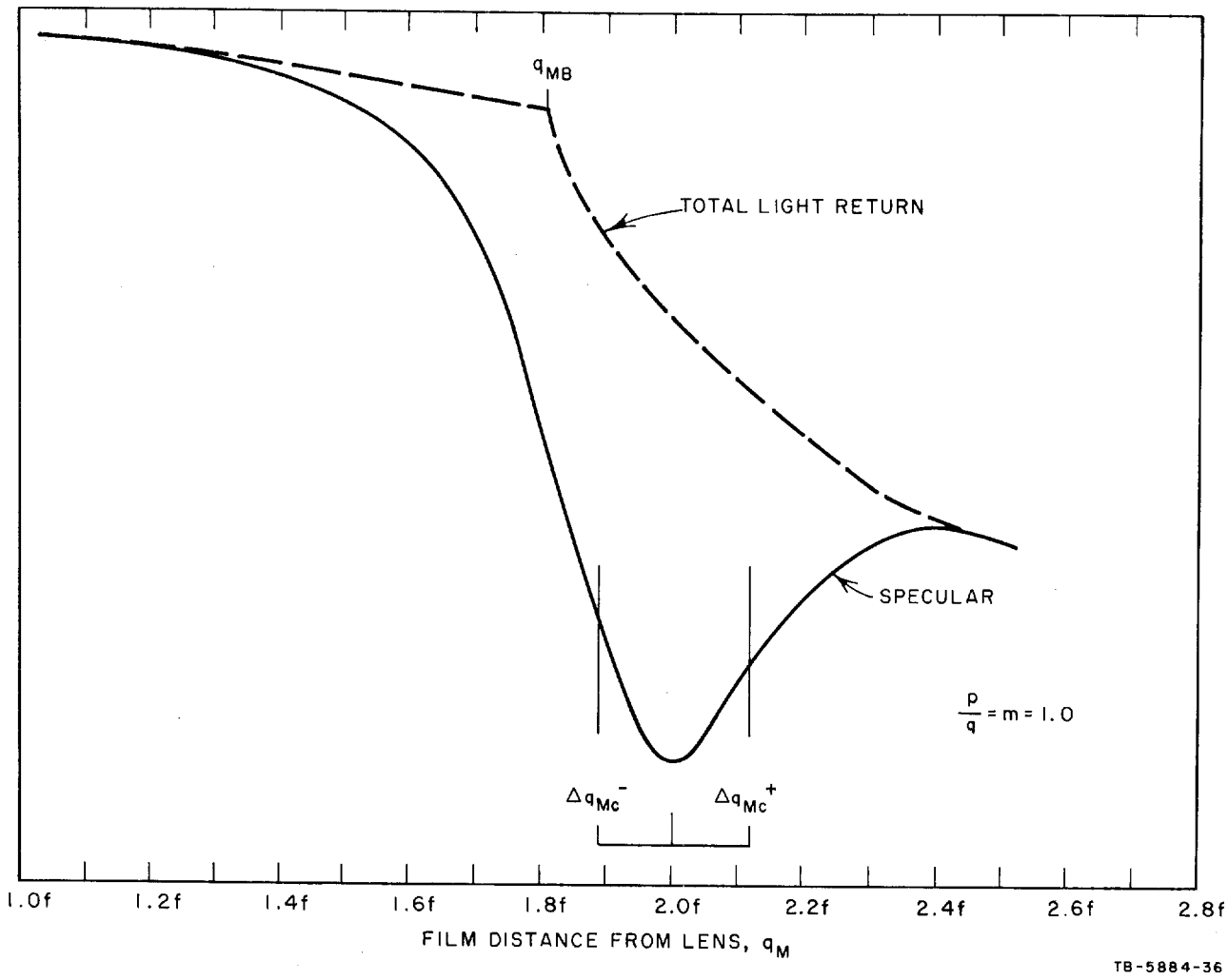

FIG. I-14 BASIC RESPONSE CURVE FOR m = 1.0

of $2\Delta q_{Mc}^+$, and this is independent of the magnification used. This validates the use of the figure corresponding to a displacement of $2\Delta q_{Mc}^+$ as the limitation-of-detection range in the positive direction of film motion.

Finally, as a method of increasing total range while at the same time maintaining the high null sensitivity, the possibility of using a mask consisting of a distributed array of small images was considered. A possible mask is shown in Fig. I-16. For this mask Δq_{Mc} is very clearly defined for the small circles making up the bulk of the mask. However, since the array of circles also has an overall circular shape,

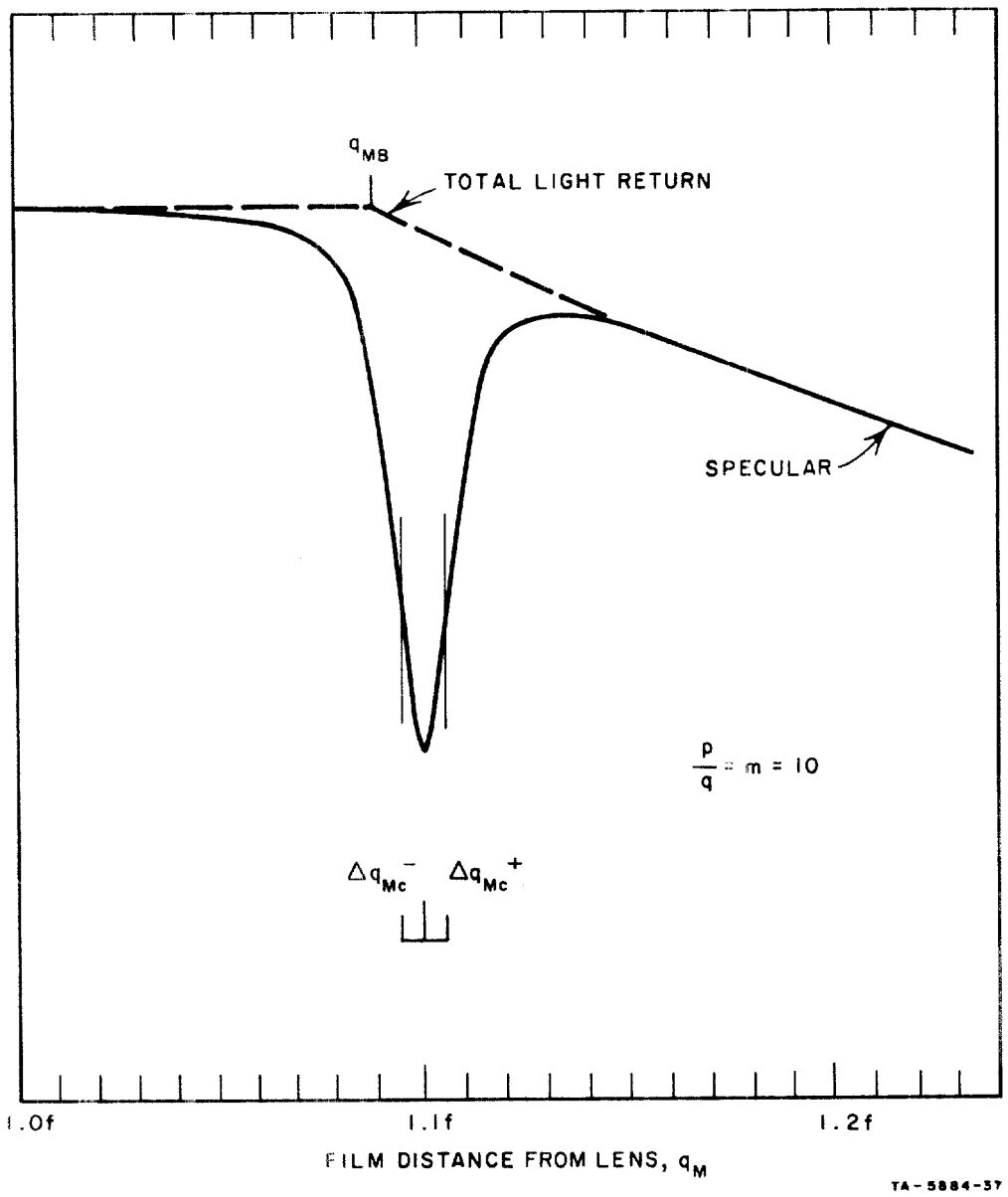

FIG. I-15 BASIC RESPONSE CURVE FOR m = 10

a $\Delta' q_{Mc}$ can be defined for the larger circle. Thus one would expect to see a combined effect which is shown in the actual response curve in Fig. I-17. Note that in this figure the null sharpness is governed by Δq_{Mc} for the small circles, while the overall range is dictated by $\Delta' q_{Mc}$ of the large circle. Where the break occurs between the two ranges is a function of the separation between the individual apertures. If

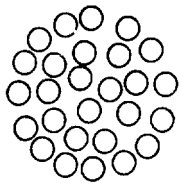

TA-5884-38

FIG. I-16 MULTIPLE MASK PATTERN

spacing is very regular and equal, then the edge transition between the two slopes will have a number of ripples due to mutual interference of the adjacent holes. The resulting ripples, if large enough, can result in false nulls which could in turn cause an error in the focus-detection

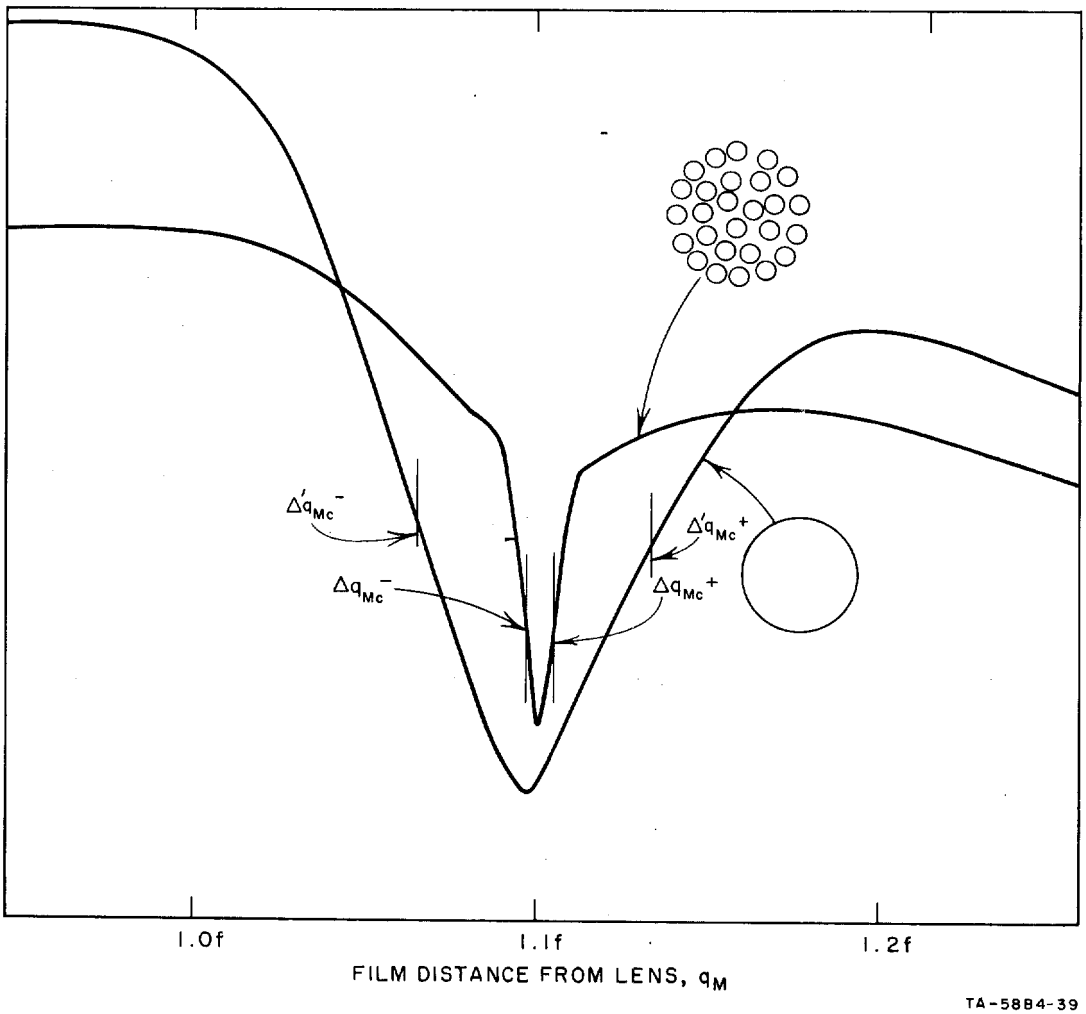

TA-5884-39

FIG. I-17 EFFECT OF MULTIPLE MASK

system. However, if the holes are irregularly distributed, these ripples will average to the relatively smooth curve shown in Fig. I-17.

E. Analysis of System Accuracy

As discussed in Sec. I-D, the experimental curves indicate that with careful design and engineering, the focus-detection system and associated lens servo should be capable of providing high precision for the focusing of the external image. This means that the mask image will be focused by the lens precisely at the front reflective surface of the film and the refocused reflected image exactly at the mask plane. With the assumption of exact focus by the focus-detection system, the following analysis will quantitatively describe resulting errors in the visual film image. Two factors cause the visual screen image for the film to be slightly out of focus when the external focus-detection image is in exact focus.

The depth of the film image behind the front surface of the film base has been measured to be between 0.003 and 0.004 inch from the sample aerial film supplied by the sponsor. This is a distance greater than the allowable depth of field for a significant portion of the operating range of a rear-projection viewer. In other applications, such as an enlarger, the externally generated image would be reflected from the emulsion side of the film rather than the other side of the film base. In these applications the dimensional difference between the surface and the emulsion will be smaller.

The second source of error results from the difference in the focal length of the projection lens in the visual wavelengths that are used to project the film image, and the focal length in the ultraviolet or infrared range used for the focus-detection system. The use of a band of wavelengths on the edge of the visual spectrum is dictated by the application to rear-projection viewers where it is desirable that the pattern used for focus detection not be visible to the viewer. In other applications where the external image would cause no interference with the system function, the focus-detection system could, if desired, operate in the visual region.

In the following analysis, the error of focus is defined as the distance from the plane of the film image to the plane where the image of the screen is focused by the visual wavelengths, when the mask and film surface are in exact focus as determined by the focus-detection system. Knowing this dimensional error between the film plane and the plane of sharp focus of the projection lens, we can compare this error with the depth of field of the projection lens at any given f-number as defined by the circle of confusion allowed for the resolution the system must have at the viewing screen.

The equation for the error as derived in Appendix A [Eq. (A-7)] has been normalized with respect to the distance L which is defined as the distance from the film surface to the projection screen. This is a constant in any given system (with the exception of the minor variations due to the motion of the film plane about the nominal value; these small changes in L would not significantly affect the resulting error values and thus are not included in this derivation). The resulting equation is

$$E_n = \frac{(q_n' + t_n)\,(1 - q_n') - f_n(1 + t_n)}{(1 - q_n') - f_n} \quad . \qquad \text{(I-11)}$$

Figure I-18 (not to scale) shows the relationship of the basic geometric parameters used in the above equation. The remaining terms are defined as follows:

$$q_n' = \frac{\gamma}{2}\left(1 - \sqrt{1 - 4\,\frac{k}{\gamma}\,f_n}\right)$$

where

$$\gamma = \frac{K'}{L} \quad ; \quad k = \frac{f'}{f} \quad ; \quad f_n = \frac{f}{L} \quad ; \quad t_n = \frac{t}{L} \quad .$$

The unprimed terms always refer to the visual lens parameters, and the primed terms refer to those lens parameters related to the lens characteristics in the wavelength band used for the focus-detection

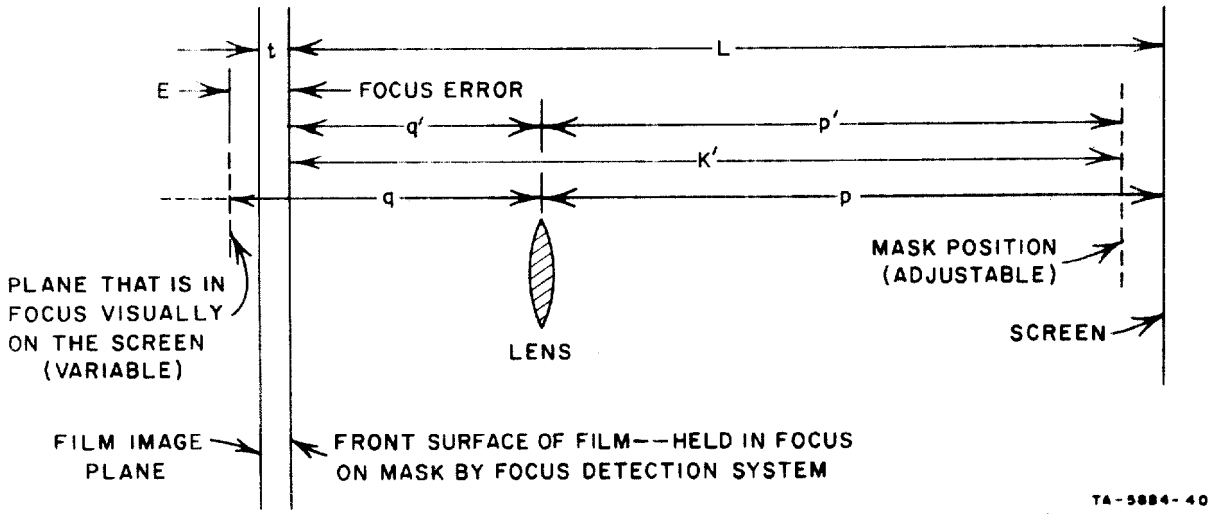

FIG. I-18 DIMENSIONS USED IN ANALYSIS OF SYSTEM ACCURACY

system. The equation and its derivation assume that the focus-detection servo adjusts precisely the lens positions so that p' is always at the film surface and q' is always at the mask.

The mask location relative to the screen is considered a constant, but subject to selection as a design parameter to be used as a means to reduce the error of the visual focus. The difference in lens focal length between the visual range and the band used for the detection system may or may not be subject to design control during the engineering of the focus-detection system. Some flexibility is provided by the choice of working the focus-detection system at either the ultraviolet or the infrared edge of the visual band.

For a selection of system parameters the error equation was computed on a digital computer and the focus error is plotted as a function of magnification for these parameters in Figs. I-19, I-20, and I-21. The magnitude of the error is plotted in terms of film-thickness units t. For the values of L, K', and γ assumed, the value of a t unit is 0.004 inch.

The error curve plotted in Fig. I-19 is for the case when the lens has the same focal length in both the visual and focus-detection wavelength bands. For this case the mask position can be located to provide

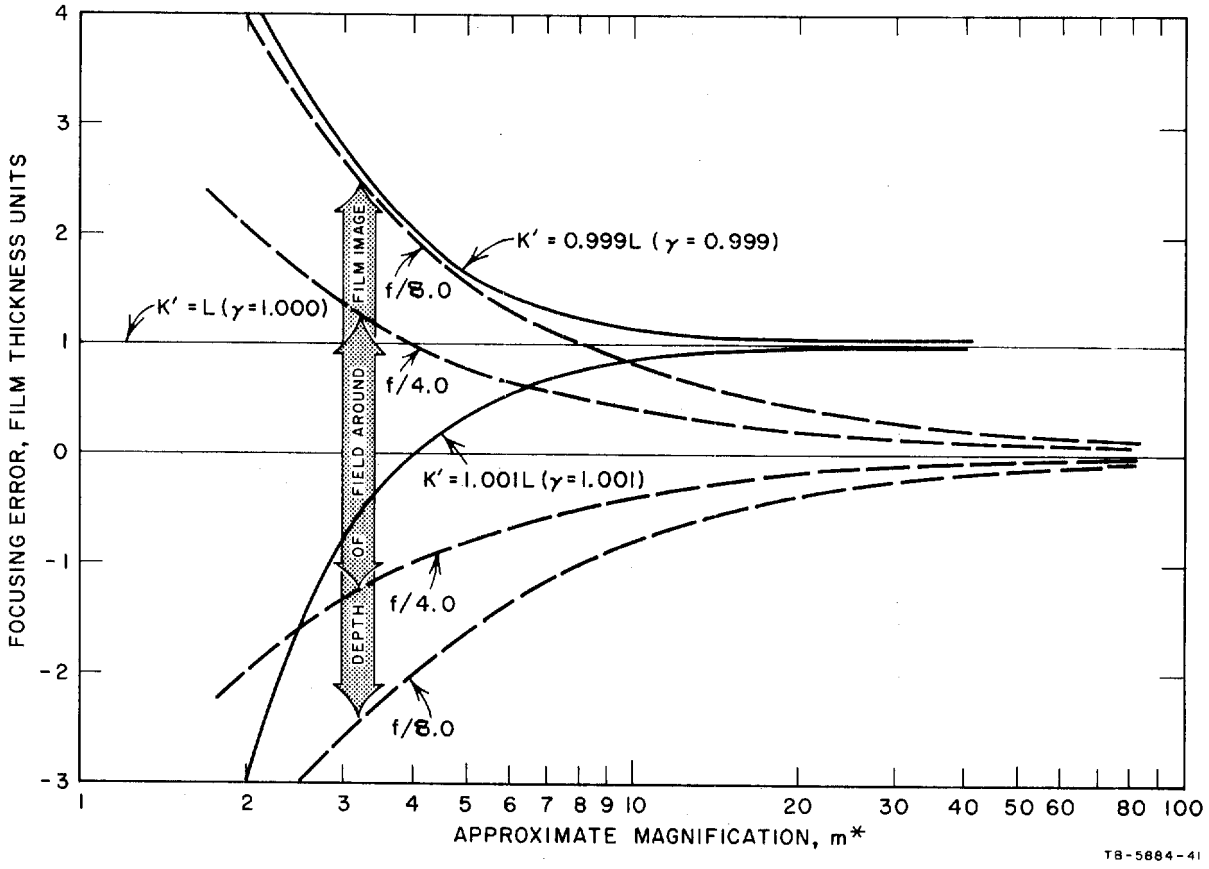

FIG. I-19 EFFECT OF CHANGE IN MASK POSITION WITH RESPECT TO SCREEN POSITION

no error for only a single magnification. For greater magnifications, the error will increase and reach a maximum value of t as m approaches infinity. At lower magnifications than the selected zero error value, the error will increase without limits.

The error curves plotted in Fig. I-20 are for the case where the mask position is held constant at the screen location ($\gamma = 1$) and the ratio of the lens focal lengths in the visual and focus-detection bands is allowed to vary ($k \neq 1$). When the lens has a different focal length in the focus-detection band than in the visual and the mask position is moved from the screen, two cases are examined:

(1) focus-detection focal length is longer than the visual and the mask is moved further from the lens than the screen ($\gamma > 1$)

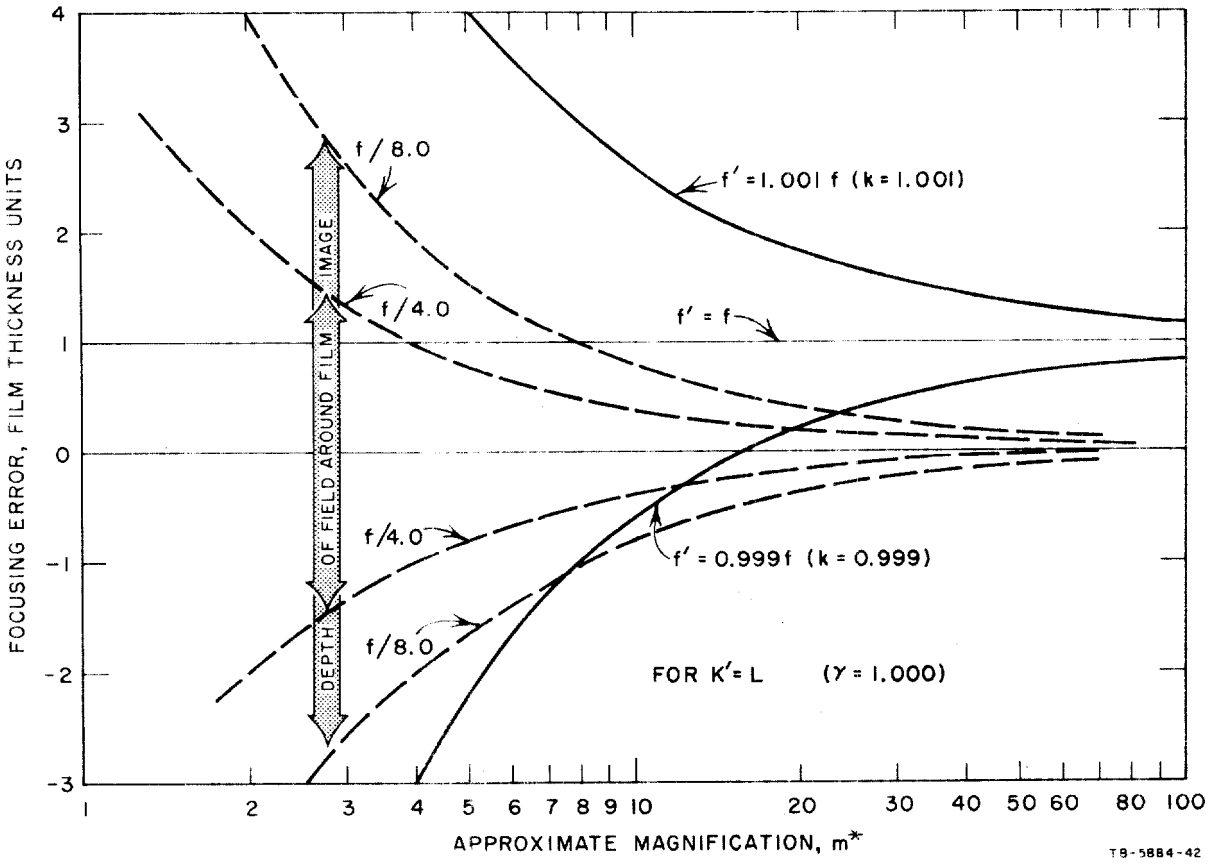

FIG. I-20 EFFECT OF DIFFERENCE IN FOCAL LENGTH FOR VISUAL AND FOCUS-DETECTION WAVELENGTHS

(2) focus-detection focal length is shorter than the visual and the mask is moved toward the lens from the screen ($\gamma < 1$).

The curves of Fig. I-21 show that zero error can be achieved for two values of magnification.

A large number of combinations of parameters γ and k were computed. The ones plotted in Fig. I-21 indicate the most promising results that were achieved over the general magnification range of 3 to 70. In a given system one or more lenses would be used to achieve this range; the freedom to select different values of k for each lens would, because of the smaller range of magnification covered by each lens, permit better error correction. The selection of the magnification at which

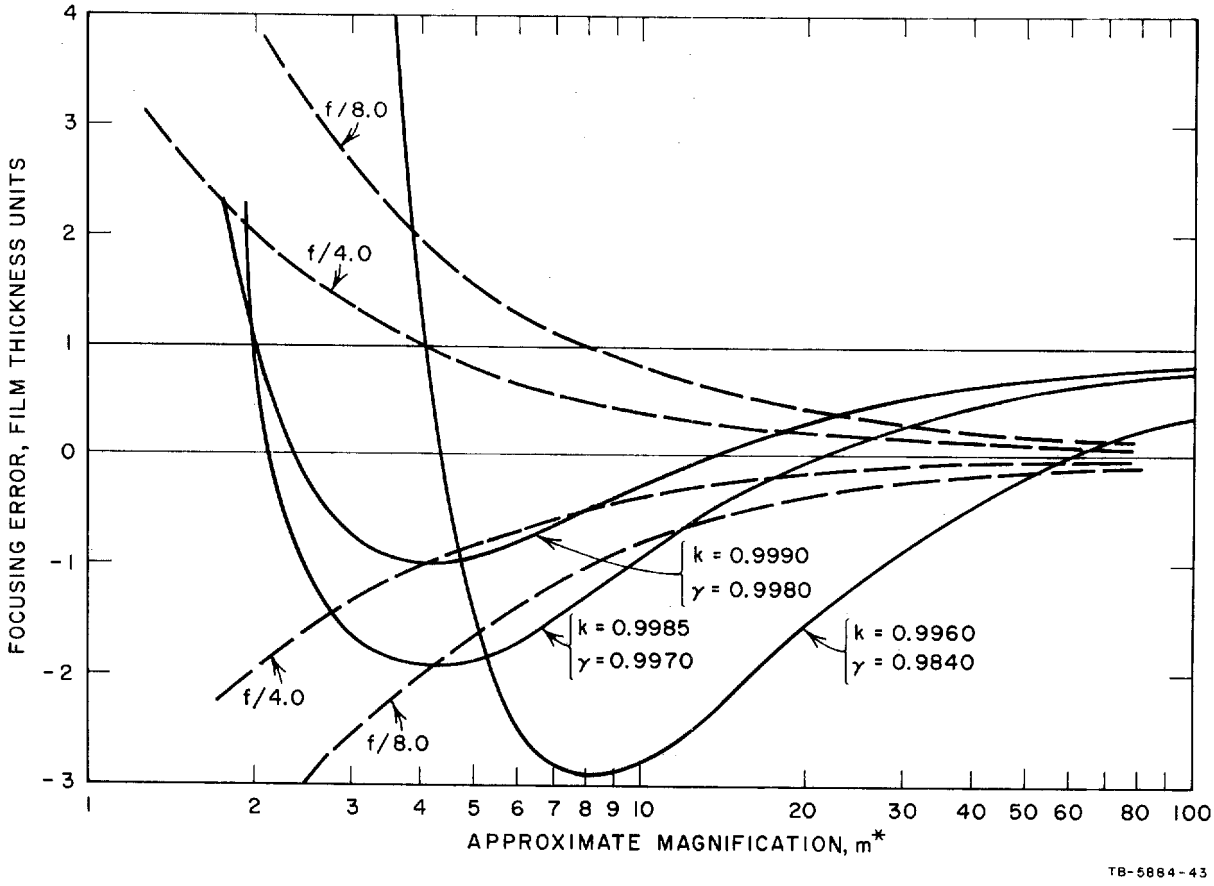

FIG. I-21 EFFECT OF COMPENSATING FOR FOCAL-LENGTH DIFFERENCE WITH A FIXED MASK-POSITION CORRECTION

zero errors are desired is a function of the system operating requirements, as is the magnitude of error permitted at other magnifications. How well these requirements can be met will depend on the freedom to select differences in focal lengths (k values) and the values required for the other system parameters (i.e., range of magnification, allowable error, lens aperture, etc.).

To relate these focusing errors to overall performance, a first-order estimate of the allowable magnitude of error was derived and is shown in Figs. I-19, I-20, and I-21 by the dotted lines for 2 values of aperture f-numbers. The requirement of a screen resolution of ten line pairs per millimeter is assumed to require a circle of confusion of 0.1 mm as the maximum allowable when referred to the screen side of the

optical system. The allowable circle of confusion referred to the film side is the circle of confusion on the screen side divided by the magnification. Therefore, at the film side the allowable circle of confusion in this system is 0.1/m millimeters.

One-half the allowable depth of field is given by the equation

$$\frac{1}{2} d = FD_c \qquad \text{(I-12)}$$

where F = lens aperture in f-stop units, and D_c = diameter of the circle of confusion.

Substituting $\frac{0.1}{m}$ for D_c in the above equation gives the allowable error between the film image and the point of exact visual focus of the lens in millimeters if the system resolution requirements are to be approximately met. The resulting equation is

$$\frac{1}{2} d = 0.1\frac{F}{m} \qquad \text{(I-13)}$$

in millimeters.

Multiplying by 10 to convert to film thickness units results in

$$\frac{1}{2} d = \frac{F}{m} \qquad \text{(I-14)}$$

in film thickness units.

A study of the error in visual focus as a function magnification in Figs. I-19, I-20, and I-21 shows that the error in visual focus cannot be kept within the required depth of field over the full magnification range of 3 to 70 when restricted to fixed values of γ. If γ is allowed to vary as a function of the magnification (physically this means moving the mask with respect to the screen) a zero error could be achieved over a wide range of magnifications. A solution of Eq. (I-11) for γ over the desired range of m with the requirement that the error be kept at zero and for a selected value of k would provide data giving the required motion of the mask in relation to the screen as a function

of magnification. The magnification is not explicit in Eq. (I-11) but is defined in terms of f_n in Appendix A.

Moving the mask as magnification is changed is worth serious consideration as a means of reducing the focusing error. The motion required need not be precise, since small errors in mask position are only second-order effects in the accuracy of focus. For example, at a magnification of three, the depth of field in the film plane for an f/4.0 lens is ±0.005 inch. Referred to the mask position the allowable error corresponding to this depth of field is m^2 times 0.005 inch or 0.045 inch. For greater magnifications, the required accuracy of mask location decreases. At m = 70, for example, the depth of field at the film for an f/4.0 lens is ±0.00023 inch. The corresponding allowable error in mask placement is (0.00023) times $(70)^2$ or 1.1 inches.

Therefore, a mechanism to move the mask as a function of magnification could be easily designed to provide for precise correction to the visual focus. Errors in the motion of the mask are only second-order effects in the focus correction. This is in contrast to the system described in Sec. I-B-1 where the open-loop lens position is controlled by a cam. In these systems the cam error must be less than the depth of the field permitted at the film throughout the operating range.

This analysis of error in the automatic focusing system using an external image reflected from the front surface of the film indicates that for low magnifications (for example m = 3 to 10), system accuracy can meet the requirements with a selected but stationary mask position. From an operational point of view, automatic focusing during the scanning mode is very desirable, since in this mode it is not possible to manually focus with sufficient speed or accuracy. If operational use of future rear-projection viewers plan significant use of static high-magnification viewing, two courses of action are suggested.

(1) During the high magnifications, when the film is stationary, the operator can use manual focusing since the images are stationary during close scrutiny. This is recommended if only occasional high magnification viewing will be performed.

(2) Incorporate mechanical coupling of the mask position with the change in magnification to achieve critical automatic focus throughout the entire range of magnifications.

F. Experimental Focus-Detection System

Figure I-22 shows schematically a breadboard system that was built and tested to confirm that the focus-detection system would work in a layout similar to a rear-projection viewer. With the pellicle mirror in the flat position, the other optical path lengths were adjusted so

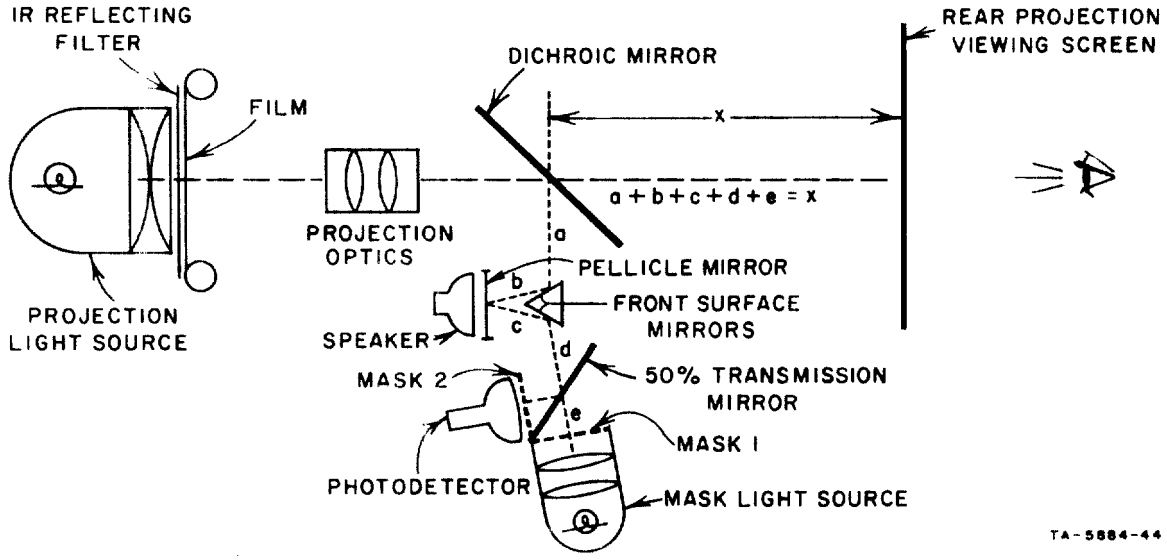

FIG. I-22 EXPERIMENTAL SYSTEM FOR SIMULATING A REAR-PROJECTION VIEWER

that mask and screen were at equal distances from the film. At the low magnifications used, the depth of field of the lens was sufficient to place the visual projection image in focus when sharp focus was indicated by the signal from the photodetector. The system employing two masks, one positive and one negative, was utilized to confirm that this approach could be easily implemented. A dielectric film reflecting filter was placed between the projection light source and the film to prevent infra-red from this source reaching the photomultiplier tube. The combination

of this infrared reflecting filter at the projection light source and an infrared pass filter placed in front of the photodetector provided sufficient separation of wavelength bands for independent operation of the photodetection system and the visual projection system.

A small audio speaker was used to vibrate the pellicle mirror to produce output sine waves from the photodetector whose frequency doubles at exact focus. When the image is out of focus, the phase indicates the direction required to correct focus.

The use of a microscope to examine the projected image at the screen position revealed sharp, critical focus as determined by viewing the grain pattern of the projected image, when the system was adjusted by visual reference to an oscilloscope showing a second-harmonic signal from the photodetector.

The laboratory tests of this breadboard confirmed that the external-image focus-detection technique could be applied to a rear-projection viewer system of the size and layout required for viewing 9-inch wide aerial film at magnifications from 3 to 10. Returned-light levels for the photodetector were more than adequate to provide an excellent signal-to-noise ratio from the photomultiplier. The use of two multilayer dielectric filters, one to exclude infrared from the projected image and the other to exclude the visible spectrum from the photodetector were more than adequate to isolate the two systems when operating at realistic illumination levels as would be required in a rear-projection viewing system.

G. Conclusions

(1) A focus detection system has been developed offering the following advantages:

(a) The system detects the actual sharpness of an image formed by the optical system in which focus is being measured.

(b) The signal from the detection system can be used to control any one of the three

basic parameters, lens position, film position, or image-plane position.

(c) The actual detection of image focus, combined with closed-loop control of any one of the basic focus parameters, permits the system to be applied to a variety of applications and equipment.

(d) The system is particularly suited to application to the dynamic focusing of the rear-projection viewer in the scanning mode at low magnifications.

(2) The results justify a continuation of work in two areas:

(a) A direct-application project in which a working prototype focus-detection unit would be engineered to an existing rear-projection viewer. The completed system could be used to measure the quantitative technical performance achieved in a real system, and the viewer could be returned to the sponsor for operational use to determine its potential functional benefits.

(b) Continuation of the basic theoretical and laboratory work to extend and refine this technique and to develop extensions for application to a variety of optical systems requiring automatic focus detection and correction. Specific areas of further study should include the extension of each design to achieve increased accuracy and range of focus detection. An investigation of three-dimensional masks and dual detectors for detecting the direction of focus error would, if successful, provide an alternative to the vibrating pellicle mirror now used for this purpose.

II THEORETICAL ANALYSIS

The purpose of this section is to develop an analytic basis for the experimental curves of Sec. I.

Suppose that we form a real image of an object, and reflect the image in a perfect mirror. The reflected image will act as a new source which is in turn imaged by the lens. If the mirror were located in the in-focus image plane, then ideally the new image (by optical reciprocity) would fall exactly on top of the original object. When the mirror is shifted along the optical axis, the position of the first real image also shifts axially, and there is a corresponding axial shift of the position of the second image with regard to the original object plane. Viewed from the object plane, the second image appears defocused, and we define this situation single defocus.

Substituting a light diffuser, such as a piece of white paper, in place of the mirror then the first image is itself defocused whenever the diffuser is outside of the image plane. The second image formed by the lens is a focused version of the first defocused image. Viewed from the original object plane we see a defocused version of the second image, and this we define double defocus. Single-defocus analysis is the most relevant here, since the total incident light returned from ordinary film is primarily specular (the film acting as a mirror) and only slightly diffuse.

A. Single Defocus

1. Basic Problems of Analysis

A mirror located in the image plane of a lens system will reflect the real image, which will in turn act as a new source to be imaged by the lens. Assuming a distortionless lens, optical reciprocity shows that the second image will fall exactly on the original object. Thus, in Fig. II-1, point P is imaged as point Q. All of the light reaching Q in incident bundle I is reflected about the normal N drawn

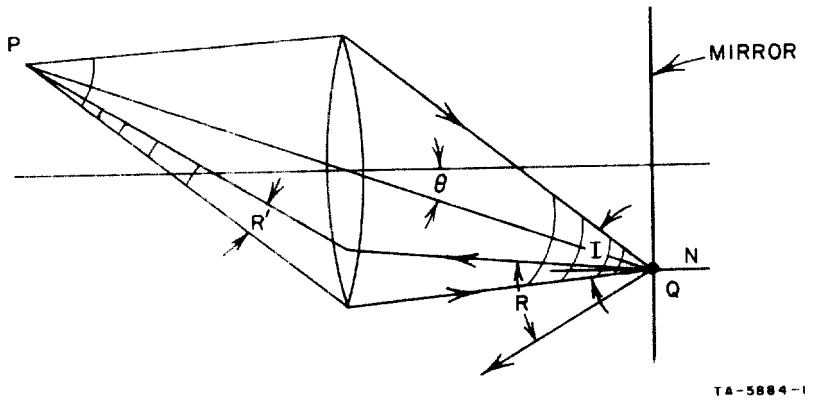

FIG. II-1 INCIDENT CONE I AND REFLECTED CONE R FROM MIRROR

to the mirror at Q. A first important effect to note is that of all the light in the reflected bundle R, only a portion R′ is actually re-imaged at point P. The remainder (R-R′) misses the lens entirely and is lost. The percentage of light lost increases with the angular displacement θ of the object.

If the mirror moves axially by an amount Δq_M (Fig. II-2) then the image of the source forms not at Q, but at Q′, a distance $\Delta q = 2\Delta q_M$ in front of the original image plane. Point Q′ is displaced from the

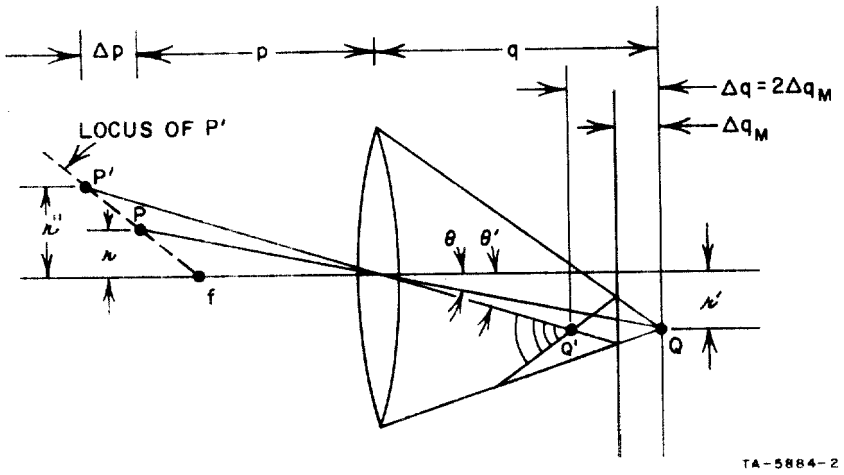

FIG. II-2 CHANGE IN MAGNIFICATION WITH MIRROR MOVEMENT Δq_M

optical axis by exactly the same amount as point Q, but since Q′ is closer to the lens, we see that the angular displacement θ′ of the image is larger than the angular displacement θ of the original image. Q′ is reimaged as P′, displaced an amount Δp from the object plane.

We can show that the change in size of the second image is such that P′ falls on a line drawn through the original point P and the intersection of the focal plane and the optical axis. Let r be the displacement of P from the optical axis. From the simple lateral magnification relation for a lens, we see that the first image Q is displaced r′ from the optical axis, where

$$r' = (q/p)r \quad . \tag{II-1}$$

As the mirror is moved, the displacement of the new image point Q′ from the axis is the same as for point Q. The moving mirror thus creates a moving point image of constant displacement r′ which is reimaged in some plane p′ = p + Δp. The displacement r′′ of the returned image is given by

$$r'' = \frac{p'}{q'}(r') = \frac{p'}{q'}\left(\frac{q}{p}\,r\right) \tag{II-2}$$

where q′ = q + Δq. From the basic lens formula

$$\frac{1}{f} = \frac{1}{p} + \frac{1}{q} \tag{II-3}$$

we readily derive the relation between p′ and q′, namely

$$q' = \frac{p'f}{p' - f} \quad . \tag{II-4}$$

Thus,

$$r'' = \left(\frac{p + \Delta p}{f} - 1\right)\frac{q}{p}\,r \tag{II-5}$$

which can be written in the alternate forms

$$r'' = r\left(1 + \frac{\Delta p}{p - f}\right) \qquad \text{(II-6a)}$$

$$r'' = r\left(1 + \frac{\Delta p}{p}\frac{q}{f}\right) \quad ; \qquad \text{(II-6b)}$$

all of the forms show that r'' is a linear function of Δp that intercepts zero (the optical axis) at $p' = f$. In other words, the final image point P' moves along a straight-line locus drawn between the original point P and a point on the optical axis at the focal length of the lens, as shown in Fig. II-2.

To express r'' in terms of Δq, we simply subtract Eq. (II-3) from the relation for the second imaging, namely

$$\frac{1}{f} = \frac{1}{p + \Delta p} + \frac{1}{q + \Delta q} \qquad \text{(II-7)}$$

from which we derive the expressions

$$\frac{\Delta p}{p} = \frac{-\,p/q}{\frac{q}{\Delta q} + \frac{p}{f}} \qquad \text{(II-8a)}$$

$$\frac{\Delta q}{q} = \frac{-\,q/p}{\frac{p}{\Delta p} + \frac{q}{f}} \quad . \qquad \text{(II-8b)}$$

Substituting Eq. (II-8a) into Eq. (II-6b) we find

$$r'' = r\left(\frac{1}{1 + \frac{\Delta q}{q}\frac{p}{f}}\right) \quad , \qquad \text{(II-9)}$$

or in terms of mirror movement $\Delta q_M = 1/2\ \Delta q$

$$r'' = r\,\frac{1}{1 + \frac{2\Delta q_M}{q}\left(\frac{p}{f}\right)} \quad . \qquad \text{(II-10)}$$

We see then that an accurate analysis of the single-defocus scheme requires attention to loss of reimaged light with increasing angular displacement θ in Fig. II-1, and the change in size of the second image, according to Fig. II-2.

2. Geometric Form for Analysis--Disk Object

Assume a large opaque sheet in the object plane with a circular cutout of diameter W that is uniformly illuminated from the rear, Fig. II-3. Assume further that the opaque sheet has a white diffusing surface facing the lens and that a photodetector monitors the total light falling onto the white surface.

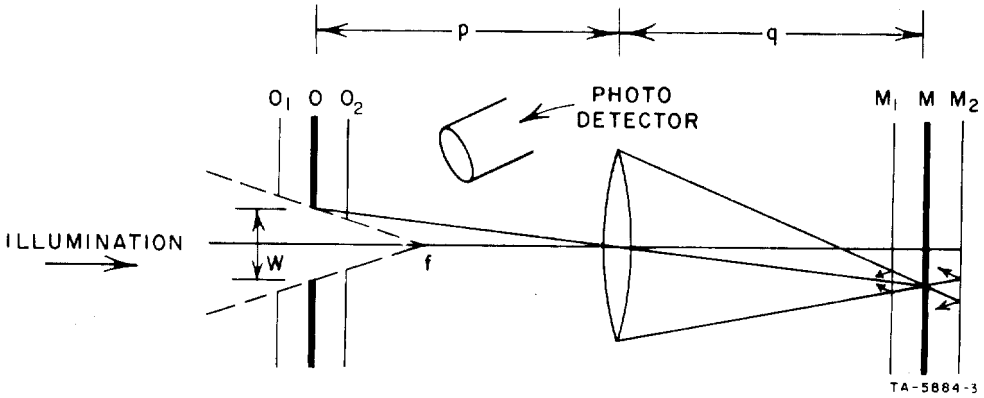

FIG. II-3 DETECTION OF INTERCEPTED LIGHT IN OBJECT PLANE

With mirror M in the image plane, the real image of the illuminated aperture is reflected by the mirror and exactly reimaged on the aperture, thus no light is reflected into the detector. If M shifts towards the lens by an amount Δq_M, to position M_1, the second image shifts an amount Δp, to position O_1, and is enlarged according to Eq. (II-6). Similarly, if M moves away from the lens to M_2, the now smaller second image shifts towards the lens to O_2. With any shift in mirror position from focus, the second image no longer matches the object, and some light reaches the detector.

What we are interested in is the magnitude of detected light as a function of mirror shift Δq_M. For purposes of analysis, we will assume that the photodetector collects all of the light intercepted by

the opaque sheet. We also are interested in how this function changes with system parameters; in particular, the magnification ratio q/p, the width W of the object, the lateral displacement of the object, and angular changes of the mirror with respect to the optical axis.

3. Preview of Analytical Steps

We see from Sec. I that the experimental curves have the general form sketched in Fig. II-4(a). We hope to understand from the analysis the reasons for the shapes of different parts of the curve, and in particular to be able to predict how the curve will vary with changes in magnification ratio (p/q) and changes in object-to-lens ratio (W/D).

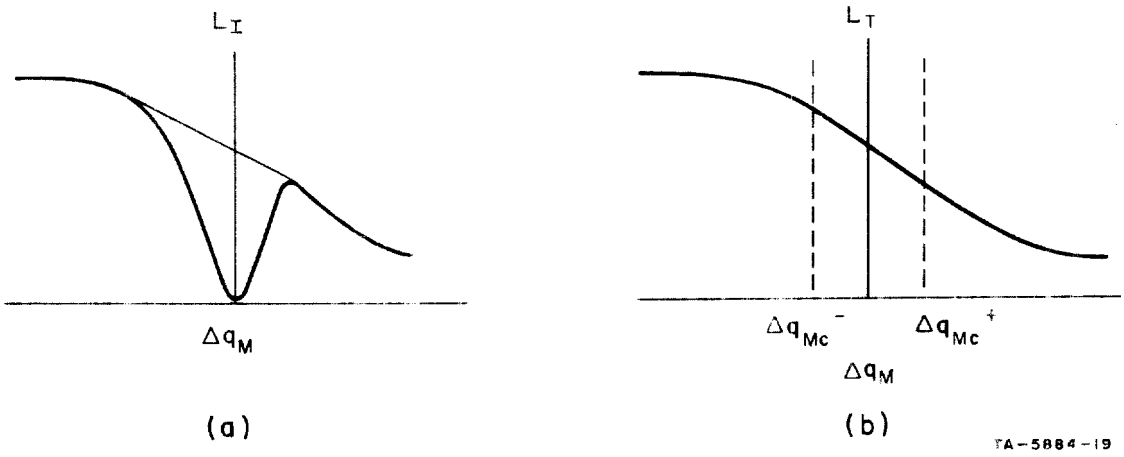

FIG. II-4 FORM OF TOTAL RETURNED LIGHT L_T AND INTERCEPTED LIGHT L_I AS FUNCTIONS OF MIRROR POSITION Δq_M

The analysis proceeds as follows: In the following two sections, we show that the total light L_T returned through the lens has the form sketched in Fig. II-4(b). For large defocus (i.e., large values of $|\Delta q_M|$), the intercepted light L_I will have the same general form, as a function of Δq_M, as the total light L_T. However, we are primarily interested in intercepted light L_I for small values of Δq_M. Of special importance is the existence of a range on either side of $\Delta q_M = 0$ for which the computation of intercepted light is relatively

simple. In Secs. II-A-6 and II-A-7, we define the value of these ranges, and in Secs. II-A-8 and II-A-9 we discuss the form of the L_I curves over these ranges.

In general we are able to predict analytically all of the prominent features of the curve of Fig. II-4(a).

4. Specular Light Loss--Point Source

We noted in connection with Fig. II-1 that some portion of the light reflected from the mirror will cross the lens plane outside the limits of the lens and therefore will be lost. What we wish to calculate here is how the proportion of light lost in this fashion varies with the magnitude of displacement of the object point from the optical axis, and also on the axial position of the mirror.

Consider a point located a distance p from the lens, and a distance r from the optical axis, Fig. II-5(a). The image of this point, which is at a distance q from the lens, will have a displacement from the optical axis of r(q/p) from Eq. II-1. The circular cone of light coming to focus at this image point is reflected by the mirror, and intersects the lens plane with a disk having exactly the same diameter as the lens but displaced from the optical axis by a distance S, where

$$S = 2r\left(\frac{q}{p}\right) \quad . \tag{II-11}$$

The light that passes back through the lens is represented by the common cross-hatched area. The magnitude of the common area A, as a function of the separation S is derived in Appendix B and plotted as the $\Delta q_M = 0$ curve in Fig. II-5(b). (The derivation in Appendix B is for two disks of arbitrary radii, (r,R) though we are concerned at the moment only with the case of equal radii, r = R). Note that A reaches zero when S = D, where D is the diameter of the lens. From Eq. (II-11) we see that the value of r, (which we call r_c) for which S = D is

$$r_c = \frac{D}{2}\frac{p}{q} \quad . \tag{II-12}$$

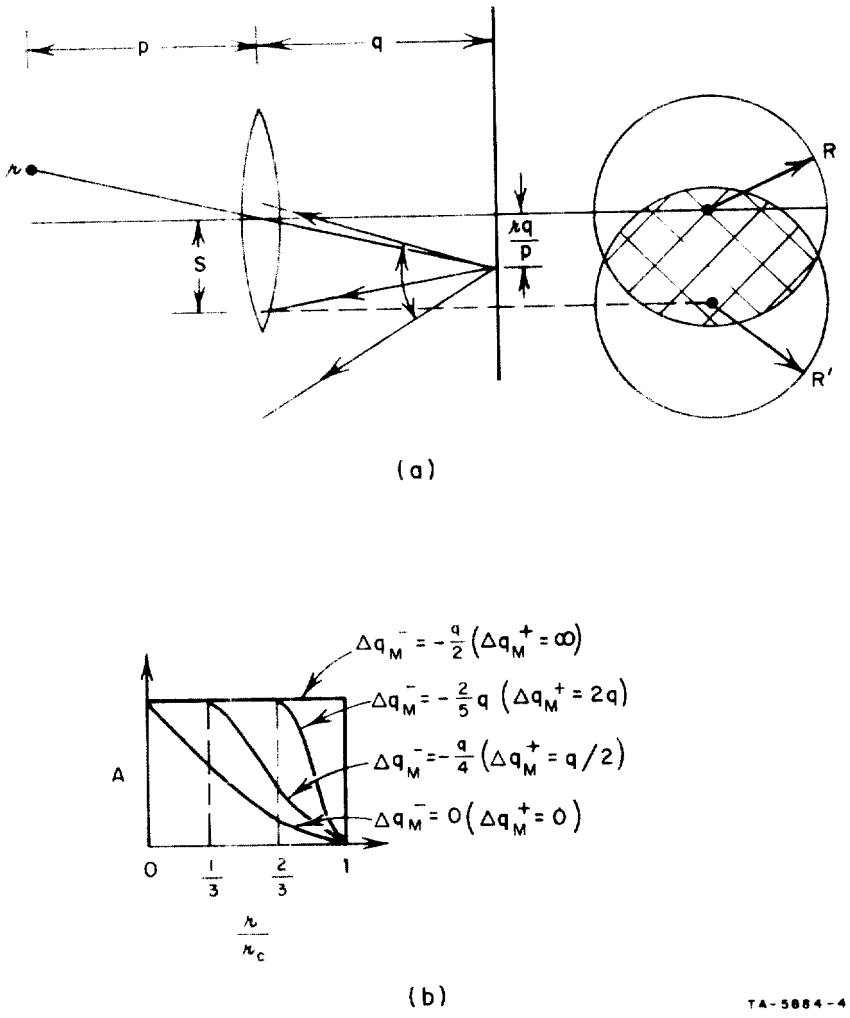

FIG. II-5 RETURNED-LIGHT DISK IN LENS PLANE
(a) Separation S of light disk and lens disk
(b) Common area A as a function of normalized object distance from lens axis, for different mirror positions

At this limiting condition the lowest ray of the focusing cone is exactly parallel to the optical axis. This ray is reflected back on itself with the remainder of the cone completely below it.

Let us consider now the effect of moving the mirror along the optical axis. With mirror movement away from the lens, the diameter of the reflected light cone in the lens plane is increased to

$$D' = D\left(\frac{q + 2\Delta q_M}{q}\right) = D\left(1 + \frac{2\Delta q_M}{q}\right) \qquad \text{(II-13)}$$

which is independent of the value of r.

For positive values of Δq_M, $D' > D$ and we have the situation of Fig. II-6(a). The common area remains constant for a lateral shift up to $S = (R' - R)$ at which point the two circles become internally

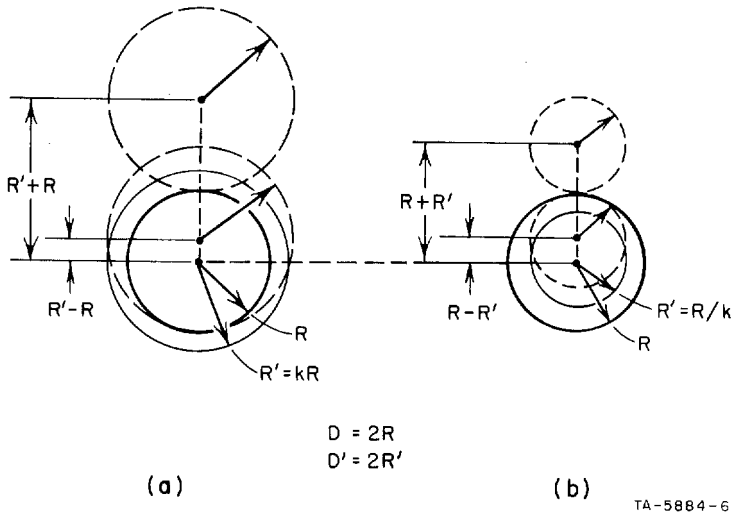

FIG. II-6 RELATIONSHIP OF LIGHT DISK AND LENS DISK WITH MIRROR OUTSIDE IMAGE PLANE
(a) Mirror beyond image plane
(b) Mirror between lens and image plane

tangent. The common area decreases monotonically for larger separations, becoming zero at $S = R' + R$ at which point the two circles are externally tangent. For negative values of Δq_M, $D' < D$, and we have the situation of Fig. II-6(b).

We can readily generalize the expression (II-11) to include the effects of different mirror positions, namely

$$S = 2r\,\frac{(q + \Delta q_M)}{p} = 2r\,\frac{q}{p}\left(1 + \frac{\Delta q_M}{q}\right) \quad . \qquad \text{(II-14)}$$

Using Eq. (II-14), we can find the value of r for which A = 0 (implying S = R + R′) by setting

$$2r\,\frac{q}{p}\left(1+\frac{\Delta q_M}{q}\right) = R + R\left(1+2\,\frac{\Delta q_M}{q}\right) \qquad \text{(II-15)}$$

or

$$r = \frac{D}{2}\,\frac{p}{q} \quad ; \qquad \text{(II-16)}$$

i.e., the same critical value r_c that we met before. This result is intuitively clear, namely that this zero overlap condition is reached when the lowest converging ray is parallel to the optical axis. The result (II-16) is true for positive and negative values of Δq_M. Thus, all A(r) curves of Fig. II-5 become zero for $r = r_c$.

We see from Fig. II-5 that each curve is labeled with two values of Δq_M. The reason is that the form of the convolution depends only on the ratio of the circle diameters. Thus, the convolution curve for a reflected circle of diameter $D' = kD$, where $k > 1$ (which occurs for positive values of Δq_M), has exactly the same shape, though not the same amplitude (we will discuss this further), as the curve for a reflected circle of diameter $D' = D/k$, which occurs for negative values of Δq_M. We can use Eq. (II-13) to find the corresponding values of Δq_M^+ and Δq_M^-, by setting

$$\frac{D\left(1+2\,\dfrac{\Delta q_M^+}{q}\right)}{D} = \frac{D}{D\left(1+2\,\dfrac{\Delta q_M^-}{q}\right)} \qquad \text{(II-17)}$$

from which we obtain

$$\frac{1}{\Delta q_M^+} + \frac{1}{\Delta q_M^-} + \frac{2}{q} = 0 \quad . \qquad \text{(II-18)}$$

The corresponding values of Δq_M^+ and Δq_M^- are shown plotted in Fig. II-7. Note that Δq_M^- has an asymptote at $(-q/2)$, at which point the reflected circle has a diameter $D' = 0$.

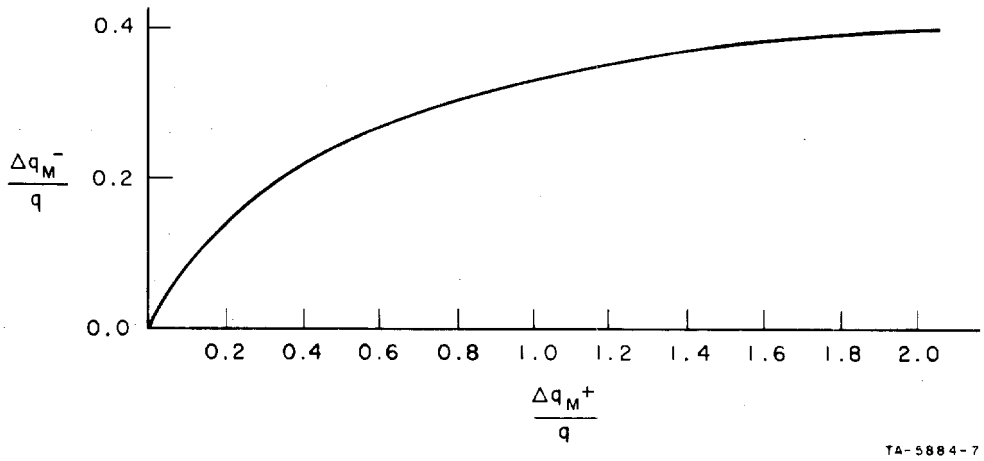

FIG. II-7 CORRESPONDING VALUES OF Δq_M^- AND Δq_M^+ LEADING TO IDENTICAL SHAPES OF A(r) CURVES IN FIG. II-5(b)

Let us next find the maximum value of r, namely r^*, over which A has its maximum value. Using Eq. (II-14) and setting $S = R - R'$, we find

$$2r^* \frac{q}{p} \left(1 + \frac{\Delta q_M^-}{q}\right) = R - \left[R \left(1 + 2 \frac{\Delta q_M^-}{q}\right)\right] \quad ; \qquad \text{(II-19)}$$

$$r^* = r_c \frac{-\Delta q_M^-/q}{1 + (\Delta q_M^-/q)} = r_c \frac{-1}{\frac{q}{\Delta q_M^-} + 1} \quad . \qquad \text{(II-20)}$$

For positive values of Δq_M, Eq. (II-19) is instead set up as $S = R' - R$, or

$$2r^* \frac{q}{p} \left(1 + \frac{\Delta q_M^+}{q}\right) = R \left(1 + \frac{2\Delta q_M^+}{q}\right) - R \qquad \text{(II-21)}$$

from which we find

$$r^* = r_c \frac{\Delta q_M^+/q}{1 + (\Delta q_M^+/q)} = r_c \frac{1}{\frac{q}{\Delta q_M^+} + 1} \quad . \qquad \text{(II-22)}$$

From Eq. (II-18) we find that Eqs. (II-20) and (II-22) yield identical values of r^* for corresponding values of Δq_M^+ and Δq_M^-. Equation (II-22) is plotted in Fig. II-8. Note that r^*/r_c approaches unity for large Δq_M^+, which from Eq. (II-18) corresponds to $\Delta q_M^- = -q/2$. As already noted, the condition $\Delta q_M^- = q/2$ corresponds to $D' = 0$ (a circle of zero diameter), for which case we should expect the convolution curve to be constant for $0 \leq r \leq r_c$, and then drop abruptly to zero, as seen in Fig. II-5(b).

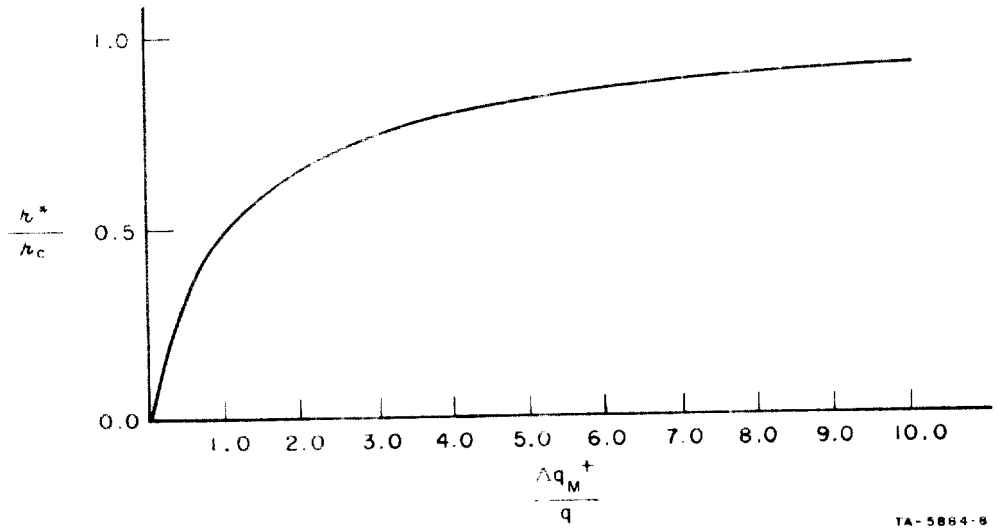

FIG. II-8 RANGE OF r OVER WHICH COMMON AREA A HAS MAXIMUM VALUE

One final point about the curves of Fig. II-5; though the A(r) curves have identical shape for corresponding values of Δq_M^+ and Δq_M^-, their amplitudes differ considerably. For r = 0, all of the reflected light is collected for negative Δq_M, since $D' < D$. For positive Δq_M, however, $D' > D$, and the proportion of collected light C is only

$$C = \left(\frac{D}{D'}\right)^2 \qquad \text{(II-23)}$$

or from Eq. (II-13),

$$C = \left(\frac{1}{1 + 2\,\frac{\Delta q_M^+}{q}}\right)^2 \qquad \text{(II-24)}$$

which is plotted in Fig. II-9. Thus the curves for positive values of Δq_M, which are noted in parentheses in Fig. II-5, have rapidly decreasing amplitudes in accordance with Fig. II-9.

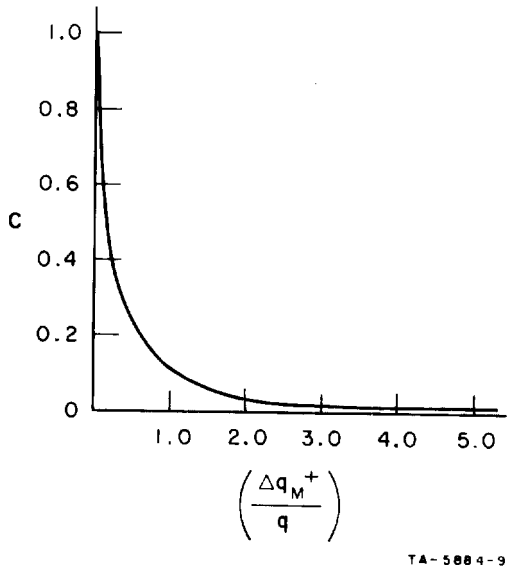

FIG. II-9 FRACTION OF RETURNED LIGHT FOR A POINT SOURCE ON AXIS AS A FUNCTION OF Δq_M^+

We have discussed the results only for $-q/2 \leq \Delta q_M \leq \infty$. We must also consider the range $-q \leq \Delta q_M \leq -q/2$; this implies mirror movements right up to the lens. In Fig. II-10(a) we illustrate the case of $\Delta q_M = -q/2$, where the reflected circle has a diameter $D' = 0$. For even larger magnitudes of Δq_M^- we see from Fig. II-10(b) that D'

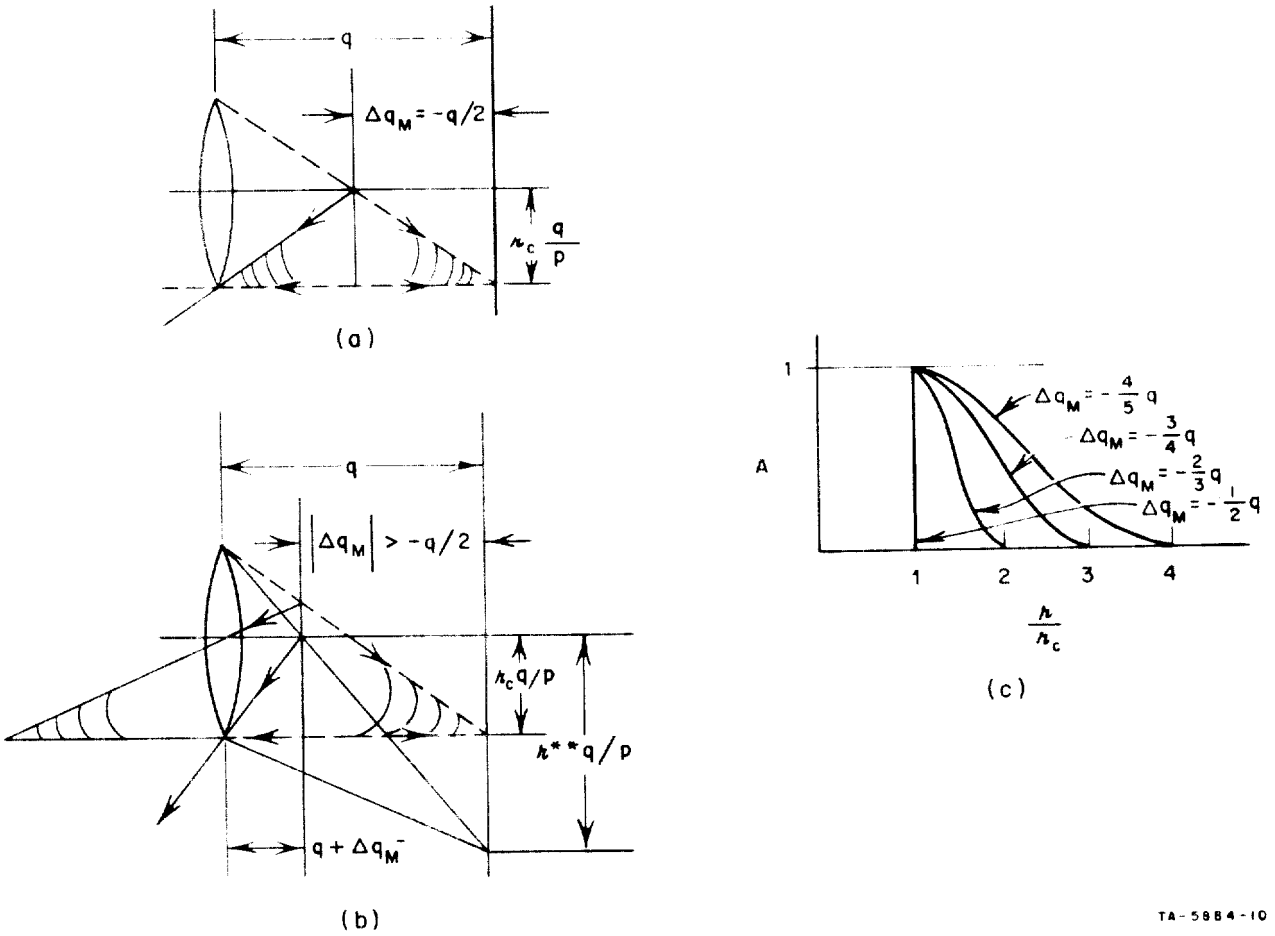

FIG. II-10 FRACTION OF RETURNED LIGHT OVER RANGE $q/2 \leq |\Delta q_M^-| \leq q$

increases in amplitude again, and that for $r = r_c$ the reflected circle again lies tangent to the lens circle, but inside the lens circle. Thus, the common area remains constant for $0 \leq r \leq r_c$ for all values of $-q \leq \Delta q_M \leq -q/2$. As r increases beyond r_c the value of A decreases until $A = 0$ at a value r^{**}, which has identically the same form as r^* in Eq. (II-20). From Fig. II-10(b) we can write

$$\frac{q + \Delta q_M^-}{D/2} = \frac{-\Delta q_M^-}{r^{**} \frac{q}{p}} \qquad \text{(II-25)}$$

or

$$r^{**} = r_c \frac{1}{\frac{q}{\Delta q_M^-} + 1} \quad . \tag{II-26}$$

The resulting curves for $-q \leq \Delta q_M \leq -q/2$ are shown in Fig. II-10(c).

5. Disk Object--Total Light Return

We have calculated the fraction of light returned from a single point source at a distance r from the optical axis, in terms of the magnification ratio p/q, lens diameter D, and mirror position Δq_M. For an object extending over an area we can integrate the fraction of light returned from each point of the object, and obtain a measure of the fraction of light from the entire object that passes back through the lens. Because of the rotational symmetry this integral is particularly simple for a circular disk object and a circular lens aperture.

The total fraction of light F passing back through the lens for a circular disk object of diameter W, Fig. II-3, is simply

$$F = \frac{1}{(\pi W^2)\ (\pi D^2)\ [\pi (R')^2]} \int_0^{W/2} 2\pi r\, A(r) dr \tag{II-27}$$

where A(r) is the fraction of light returned from a point source located a distance r from the optical axis. The function $F(\Delta q_M)$ has the general form shown in Fig. II-4(b); a total fraction of returned light that is less than unity at perfect focus ($\Delta q_M = 0$), increasing to unity at some value of Δq_M^-, and decreasing monotonically with increasing Δq_M^+. The function F reaches unity at that value of Δq_M^- for which all of the light is returned for all values of r up to r = W/2, which we find from Eq. II-20 to be

$$\left(\frac{\Delta q_M^-}{q}\right) = -\left(\frac{1}{\frac{D}{W}\frac{p}{q} + 1}\right) = -\frac{\alpha}{1+\alpha} \tag{II-28}$$

where we substitute α for the common expression W/D q/p. Thus all curves start at unity for sufficiently large Δq_M^- and monotonically decrease for increasing Δq_M^+. But for sufficiently large Δq_M^+, all

curves again become identical in shape. This occurs at that value of Δq_M^+ for which the lens is completely surrounded by the reflected circle for all values of r up to r = W/2. To find this value we recall the relations

$$R' = R\left(1 + 2\frac{\Delta q_M^+}{q}\right) \qquad \text{(II-13)}$$

$$S = 2r\frac{q}{p}\left(1 + \frac{\Delta q_M^+}{q}\right) \quad . \qquad \text{(II-14)}$$

The critical value occurs where $S = R' - R$, for $r = W/2$,

$$2\left(\frac{W}{2}\right)\frac{q}{p}\left(1 + \frac{\Delta q_M^+}{q}\right) = 2R\left(\frac{\Delta q_M^+}{q}\right) \qquad \text{(II-29)}$$

or

$$\frac{\Delta q_M^+}{q} = \frac{1}{\frac{Dp}{Wq} - 1} = \frac{\alpha}{1 - \alpha} \quad . \qquad \text{(II-30)}$$

Thus, for all $(\Delta q_M^+/q) \geq \alpha/(1 - \alpha)$ the fraction of light returned is identical for all points of the object, and therefore for the object as a whole, and the resulting curve should have the same shape as that of Fig. II-9 for a single point source.

We are primarily interested, however, in the magnitude of intercepted light L_I as a function of Δq_M. We know that this function is zero (at least ideally) at $\Delta q_M = 0$, rising on either side of $\Delta q_M = 0$. But because the total amount of returned light decreases monotonically with Δq_M, we can expect that $L_I(\Delta q_M)$ would have the form sketched in Fig. II-4(a), as actually found in the curves of Sec. I.

6. Defining the Critical Values Δp_c^+ and Δq_{Mc}^-

In the last section, we calculated the total amount of light returned through the lens. We concentrate now on the more complex

problem of the total light intercepted outside of the disk object, which is the output measure that we are really interested in.

Consider a point r on the disk object, which has a diameter W. This point images in the q-plane, a distance r (q/p) from the optical axis, Fig. II-11. If the mirror moves towards the lens by an amount

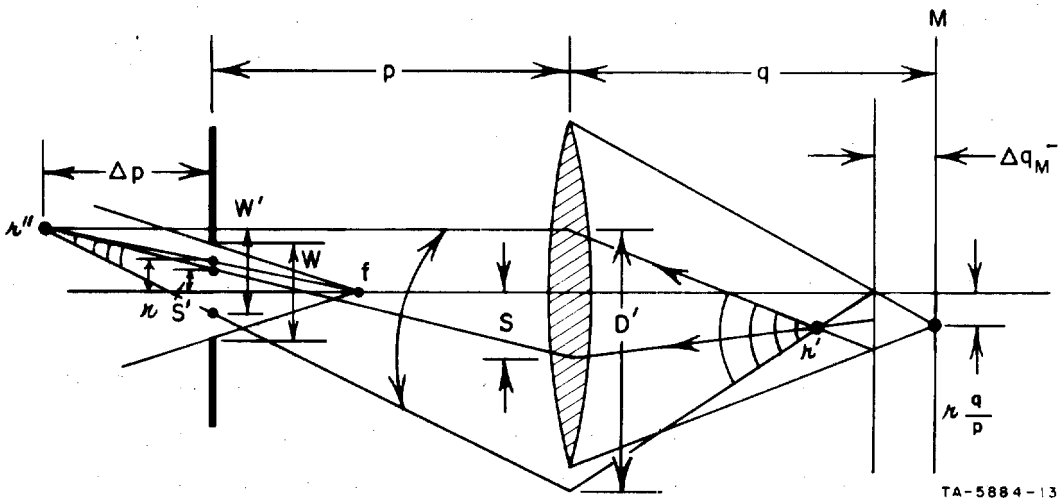

FIG. II-11 POINT SOURCE r REIMAGING AT r": CAUSING A LIGHT DISK OF DIAMETER W' IN OBJECT PLANE WITH CENTER AT DISTANCE S' FROM AXIS

Δq_M^-, then the point image moves ($2\Delta q_M^-$) towards the lens to point r′, and the cone radiating through r′ forms a disk of diameter D′ in the lens plane, whose center is displaced a distance S from the axis [see Eqs. (II-13) and (II-14)]. If S > R - R′ then part of the R′ disk is lost outside of the lens [Fig. II-12(a)]. This truncated cone in turn images at point r″, which as we saw earlier lies along a locus drawn through the object point r and the focal point f. As this truncated cone passes the object plane (the p-plane) some of the light is intercepted beyond the edge of the original disk, namely the cross-hatched region in Fig. II-12(b). If the imaging cone were a pure circular disk, the fraction of intercepted light would be easily calculated. However, if the focusing cone is sufficiently truncated, then the intercepted

light is reduced by the darkened areas A and A′ in Fig. II-12(b), and precise calculation is difficult.

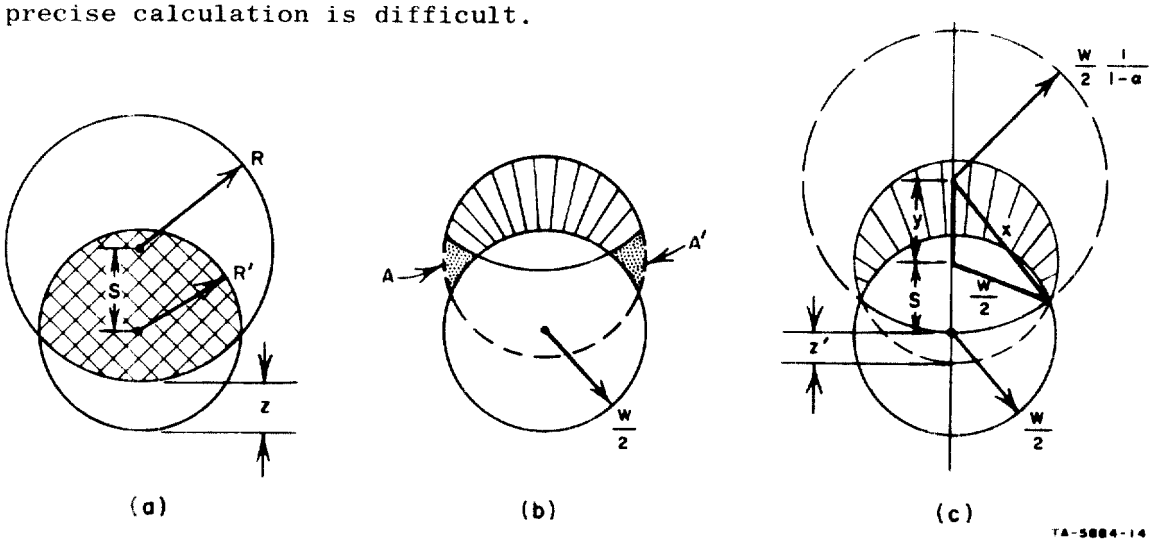

FIG. II-12 RELATIONSHIP OF OBJECT DISK AND RETURNED-LIGHT DISK TRUNCATED BY LENS

Quite fortunately there exists a particular value of mirror movement, Δq^{-}_{Mc}, and corresponding value Δp^{+}_{c}, such that if $\Delta q^{-}_{Mc} \leq \Delta q_M \leq 0$, the truncation can be neglected without error in calculating total intercepted light. We show in Appendix C that at the limit $\Delta q_M = \Delta q^{-}_{Mc}$ the truncation points just reach the disk rim as in Fig. II-12(c), so that the areas A and A′ of Fig. II-12(b) are zero.

Because of the closed-loop nature of our automatic focus-control system, we are not really concerned with the exact shape of the $L_I(\Delta q_M)$ curve on both sides of $\Delta q_M = 0$. However, we are very concerned with its width, since this defines the operating range of the servo system. It turns out that the Δq^{-}_{Mc} value gives a good measure of the range, the curve being approximately linear for $0 \leq \Delta q \leq \Delta q^{-}_{Mc}$ and falling off for $\Delta q_M > \Delta q^{-}_{Mc}$. The Δq^{-}_{Mc} points are marked on all of the experimental curves of Sec. I.

We can define a mirror position Δq^{+}_{Mc} (and corresponding value Δp^{-}_{c}) which also gives an estimate of operating range for $\Delta q_M > 0$. But whereas specular light loss beyond the lens is ineffective over the range $0 \leq \Delta q_M \leq \Delta q^{-}_{Mc}$ we will see that it does have an effect over the range $0 \leq \Delta q_M \leq \Delta q^{+}_{Mc}$.

To find the critical value Δp_c^+ let r = 0 in Fig. II-11. Now as the mirror moves towards the lens, we have two effects. First, the image point moves in a $+\Delta p$ direction along the optical axis. Second, the intercepted cone radius R' decreases so that $R' < R$. At some value of Δq_M^-, the geometry is such that the intercepted disk diameter in the p-plane exactly matches the object diameter; that is, the converging cone has diameter W in the object plane (p-plane). This condition is shown in Fig. II-13(a) (the cone from C_2 has a width W in the object plane) and is described by the relation

$$\frac{D'}{p + \Delta p_c^+} (\Delta p_c^+) = W \quad . \tag{II-31}$$

Substituting Eqs. (II-13) and (II-7), and noting that $\Delta q = 2q_M$, we find

$$\frac{\Delta p_c^+}{p} = \frac{1}{\frac{D}{W} - \frac{q}{f}} \tag{II-32}$$

or, equivalently, using Eq. (II-8a),

$$\frac{\Delta q_c^-}{q} = - \alpha \quad . \tag{II-33}$$

Note that because p and q are defined as positive in the direction away from the lens, a $(+\Delta p)$ corresponds to a $(-\Delta q)$ and vice versa.

For small Δp only the light from the edge of the disk contributes intercepted light. The zone of contribution increases monotonically with Δp. When $\Delta p = \Delta p_c^+$, the zone of contribution just reaches to the center of the disk. This is one way to interpret the significance of Δp_c^+.

Let us consider an alternate derivation and interpretation of Δp_c^+ [Fig. II-13(a)]. Consider the center C_1 of the disk in the object plane. Only when Δp_c reaches the magnitude Δp_c^+ is there a contribution at C_1 from every cone focusing on the disk in the Δp image plane.

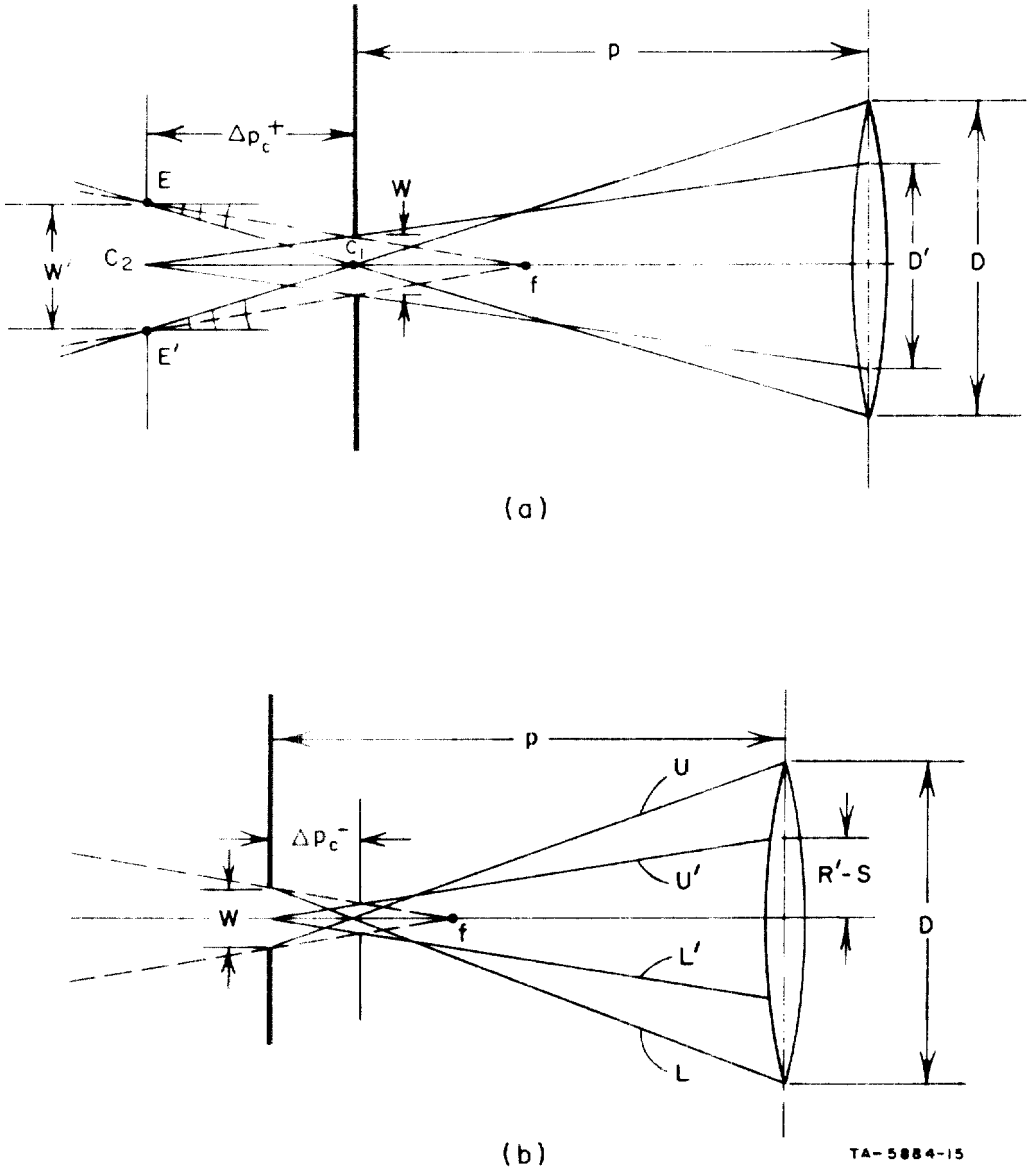

FIG. II-13 GEOMETRICAL CONFIGURATION AT CRITICAL VALUES Δp_c^+ AND Δp_c^-

Consider the extreme cones E and E′ from the edge of the disk. Substituting $\Delta q_{Mc}^-/q = 1/2\ \Delta q_c^-/q = -\alpha/2$ into Eqs. (II-13) and (II-14), we find

$$R' = R\ (1 - \alpha) \qquad \text{(II-34)}$$

$$S = R\alpha\ (2 - \alpha) \qquad \text{(II-35)}$$

from which we determine

$$S + R' - R = R(\alpha - \alpha^2) \qquad \text{(II-36)}$$

which is positive since $\alpha < 1$ in all cases of interest to us. In other words $S + R' > R$ so that the cones to the edge points extend beyond the lens. Therefore the extreme rays to E and E′ emanate from the edge of the lens. For these extreme rays to cross at the center C_1 of the disk, we must satisfy the relation

$$\frac{D}{P} = \frac{W'}{\Delta p_c^+} \quad . \qquad \text{(II-37)}$$

Substituting Eq. (II-6b) for W′, we again find the result to be Eq. (II-32) for Δp_c^+ which demonstrates the alternate derivation.

7. Defining the Critical Values Δp_c^- and Δq_{Mc}^+

As the mirror moves away from the lens in the Δq_M^+ direction, the image moves towards the lens in the $-\Delta p$ direction. As we did in the previous section for Δp_c^+, we can find a critical value Δp_c^- from the following geometric ratio in Fig. II-13(b),

$$\frac{D}{p + \Delta p_c^-} = \frac{W}{-\Delta p_c^-} \qquad \text{(II-38)}$$

which in effect states that the reimaging cone from the center of the disk object, which comes to focus in the center of the image in the Δp_c^- plane (defined by extreme rays V and L), creates a blur circle in the object plane whose diameter is equal to the disk diameter, namely W. (Note that Δp_c^- will be a negative quantity.) Equation (II-38) can be put in the form

$$\frac{\Delta p_c^-}{p} = -\frac{W}{D + W} \qquad \text{(II-39)}$$

which, by means of Eq. (II-8b), we can convert to the Δq system:

$$\frac{\Delta q_c^-}{p} = -\frac{-q/p}{\frac{p}{\Delta p_c^-} + \frac{q}{f}} = \frac{\alpha}{1-\alpha} \qquad \text{(II-40)}$$

or

$$\frac{\Delta q_{Mc}^+}{q} = \frac{\alpha/2}{1-\alpha} \quad . \qquad \text{(II-41)}$$

For the sake of completeness, we show that the second type of derivation used in the previous section for Δq_{Mc} can be used for Δq_{Mc}^+ as well. In this case, we ask that each cone coming to focus in the Δp_c^- plane contribute a ray at the center of the object in the $\Delta p = 0$ plane. Let us consider the cones coming to the edge of the image in the Δp_c^- plane [Fig. II-13(b)]. In particular, we consider the extreme ray U' which represents the topmost ray in the lens plane of the returning cone. In this case, where the mirror is moving away from the lens, the intercepted disk in the lens plane is larger than the lens disk (i.e., $R' > R$). The uppermost ray would occur at a distance R' above the axis if there were no displacement of the disk, but with a shift S the uppermost ray is a distance $(R' - S)$ above the axis.

From Fig. II-13(b) we see that $(R' - S)$ must satisfy the following geometric condition

$$(R' - S) = \frac{W'/2}{-\Delta p_c^-}\, p \qquad \text{(II-42)}$$

where W' is the image size in the Δp_c^- plane. Using Eq. (II-6b) for W', Eq. (II-42) takes the form

$$(R' - S) = -\frac{W}{2}\left(\frac{p}{\Delta p_c^-} + \frac{q}{f}\right) \qquad \text{(II-43)}$$

or in terms of Δq_c^+, using Eq. (II-8a),

$$(R' - S) = \frac{W}{2}\left[\frac{q}{\Delta q_c^+}\,\frac{q}{p}\right] = \frac{D}{2}(\alpha)\,\frac{q}{\Delta q_c^+} \quad . \qquad \text{(II-44)}$$

Now, using Eqs. (II-13) and (II-14), we can evaluate $R' - S$ as

$$R' - S = R\left(1 + \frac{\Delta q_c^+}{q}\right) - 2R\alpha\left(1 + \frac{1}{2}\frac{\Delta q_c^+}{q}\right) . \qquad \text{(II-45)}$$

Equating Eqs. (II-42) and (II-45), we can solve for Δq_c^+, which is identical to Eq. (II-4).

8. Intercepted Light Over Range $0 \leq \Delta p \leq \Delta p_c^+$

We have already noted that the exact shape of the intercepted light curve is not too important in the region about $\Delta q_M = 0$. However, we can readily demonstrate the ease of computation in case it should be necessary to compute this function.

For any given mirror position we can evaluate L_I in the form

$$L_I = \int_o^{W/2} 2\pi r I(r) dr \qquad \text{(II-46)}$$

assuming a disk object of diameter W, where I represents the fraction of the final intercepted light from a point source within W, a distance r from the axis.

The intercepted light I is generally a complicated function of r because of the two-step process of (1) truncation by the lens of the returning light cone; and (2) intersection of the smaller truncated disk with the original object. But a great simplification is achieved over the range $0 \leq \Delta p \leq \Delta p_c^+$ because the truncation has no effect on the calculation, as we show in Appendix C. Over this range, then, I(r) involves only the convolution of the intercepted cone disk with the object disk.

The convolution of two circles involves three parameters, namely the radii of the two disks and their separation. The object disk has a diameter W. The intercepted disk has a diameter W', where from Fig. II-11

$$W' = D\frac{\Delta p}{p + \Delta p} \qquad \text{(II-47)}$$

or, using Eq. (II-13)

$$W' = D \left(1 + \frac{\Delta q}{q}\right) \frac{\Delta p}{p + \Delta p} \quad . \tag{II-48}$$

Substituting Eq. (II-8b), Eq. (II-48) becomes

$$W' = D \frac{1}{\frac{p}{\Delta p} + \frac{q}{f}} \quad . \tag{II-49}$$

As for the separation distance S', from Fig. II-11 we can write

$$S' = r'' - \frac{S + r''}{p + \Delta p} \Delta p \tag{II-50}$$

which, with Eqs. (II-6b) and (II-14) can be manipulated to the form

$$S' = r \frac{\frac{p}{\Delta p} + 1}{\frac{p}{\Delta p} + \frac{q}{f}} \quad . \tag{II-51}$$

In summary then we have the relations:

$$\left.\begin{aligned} I &= I(W, W', S') \quad , \\ W' &= D \frac{1}{\frac{p}{\Delta p} + \frac{q}{f}} \quad , \\ S' &= r \frac{\frac{p}{\Delta p} + 1}{\frac{p}{\Delta p} + \frac{q}{f}} \quad . \end{aligned}\right\} \tag{II-52}$$

We can use Eq. (II-8a) to convert the expressions for W' and S' into functions of Δq:

$$W' = -\frac{Dp}{q}\frac{\Delta q}{q} = -\frac{W}{\alpha}\frac{\Delta q}{q} \quad ,$$
$$S' = r\left(\frac{\Delta q}{q} + 1\right) \quad . \qquad \text{(II-53)}$$

Thus, for each value of Δq, W, and W' are fixed, and we can integrate Eq. (II-46) since for each value of r we have a unique value of S' and can readily evaluate I (W, W', S'). We must include a normalization factor to account for the fact that as the blur circle in the object plane changes size, the average intensity varies inversely as the square of its diameter. Thus the expression for I must contain the factor $1/[(\pi/4)\ (W')^2]$.

9. Intercepted Light Over Range $0 \leq \Delta p \leq \Delta p_c^-$

For negative Δp the return disk in the lens plane is larger than the lens disk and, in the range of interest here, does not completely illuminate the lens disk. In Appendix D we show that if the light returning through the lens is treated as coming from an illuminated lens disk, but with a small truncated section (i.e., the part not illuminated in the first place by the returning light cone) then the same conclusion holds over the range $0 \leq \Delta p \leq \Delta p_c^-$ as over the range $0 \leq \Delta p \leq \Delta p_c^+$; namely, that any light in the truncated section would have passed through the object aperture anyway and therefore need not be accounted for in computing the intercepted light.

For the negative range of Δp (or positive range of Δq) we can set up an integral for the intercepted light L_I in the same form as Eq. (II-46), namely

$$L_I = \int_0^{W/2} 2\pi r\ I(r)dr \quad . \qquad \text{(II-54)}$$

To evaluate I(r), which is a simple convolution of two disks, we must know the two disk diameters and their separation. The convolution is in the object plane, so again we have the object disk of diameter W for one of the disks. The second disk is a blur disk of diameter W',

which is seen from Fig. D-1 (in Appendix D) to have the form

$$W' = D \frac{-\Delta p^-}{p + \Delta p^-} \quad . \tag{II-55}$$

The separation S' of these two disks as we again see from Fig. D-1, has the form

$$S' = r \frac{p}{p + \Delta p^-} \quad . \tag{II-56}$$

Using Eq. (II-8a) these equations can be converted to the Δq system as

$$\left.\begin{aligned} W' &= \frac{W}{\alpha} \frac{1}{1 + \frac{q}{\Delta q^+}} \quad , \\ S' &= r \frac{\left(\frac{q}{\Delta q} + \frac{p}{f}\right)}{\frac{q}{\Delta q} + 1} \quad . \end{aligned}\right\} \tag{II-57}$$

Thus, for each value of Δq, W, and W' are fixed and we can integrate Eq. (II-54) since for each value of r we have a unique value of S' and can readily evaluate $I(W, W', S')$. Again, as in the Δp^+ range, we must include a normalizing factor in the expression for I, namely $1/[(\pi/4)\ (W')^2]$, in order to give the proper weight to the common area of W and W' in terms of light intensity.

However, another important normalizing factor is needed in the Δp^- range that was not required in the Δp^+ range. In the present derivation we treat the return light cone from the lens as arising from the lens disk itself (with a small "truncated," but really not illuminated, sector). However, the light intensity over the lens disk itself varies as $(D/D')^2$, which from Eq. (II-13) has the form

$$\left(\frac{1}{1 + \frac{\Delta q}{q}}\right)^2 \quad . \tag{II-58}$$

This factor, which depends only on the value of Δq, is independent of r and therefore can be factored outside of the integral in Eq. (II-54). If it were not for this factor, the $L_I(\Delta q)$ curves would tend to be similar over the ranges $0 \leq \Delta q \leq \Delta q_c^+$ and $0 \leq \Delta q \leq \Delta q_c^-$. This extra factor tends to bend the curve over in the former range, as Δq increases, and we therefore understand the experimentally found asymmetry in these two ranges.

B. Double Defocus

With a diffusing surface instead of a specular reflector, the analysis for intercepted light as a function of Δq_D (the position of the diffusing surface) is different in detail than with the mirror. To illustrate, consider again a cut-out disk of diameter W, at a distance p from the lens, with an image distance q. If the diffuser moves axially by an amount Δq_D, then a blurred image appears on the diffusing surface. (Movement of the mirror simply caused an axial shift of the in-focus image.) Light re-emitted from the diffuser is reformed in an in-focus version (in some plane $p + \Delta p$) of the out-of-focus image; see Fig. II-14.

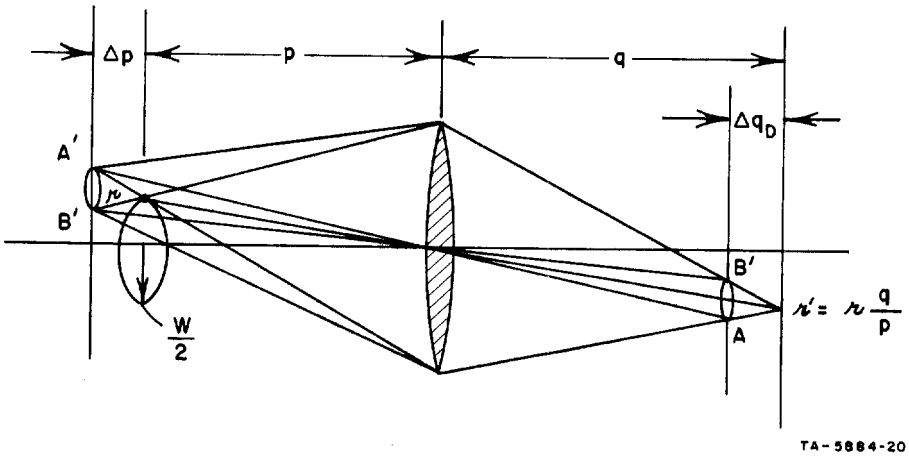

FIG. II-14 USE OF DIFFUSER INSTEAD OF MIRROR IN IMAGE PLANE

Consider a single point on the disk object, in particular the uppermost point r of the disk. Light from point r focuses in the image

plane at r′. Movement of the diffuser by Δq_D results in a blurred disk. Light reradiated in turn from each point of this blur disk tends to refocus in the p + Δp plane. Consider the upper and lower points B and A of the blur disk. These tend to reimage as points B′ and A′ in the p + Δp plane. Now consider the light intercepted outside of the object disk in the p-plane. We see from the figure that in the p-plane the intercepted disk to B′ is externally tangent to the object disk, and the intercepted disk to A′ is internally tangent, so that the entire cone converging on A′ is intercepted, whereas none of the converging cone to B′ is intercepted. It is clear that to find the total intercepted light, we could perform the convolution for the entire disk.

We do not pursue the analysis of double defocus further here, however; first, because as we noted earlier it is not particularly relevant to this application, and second because there is at least some rudimentary analysis along these lines available.*

STAT

APPENDIX A

DERIVATION OF FOCUS ERROR EQUATION

APPENDIX A

DERIVATION OF FOCUS ERROR EQUATION

The distance between the plane of the real image on the film and the plane which is in focus on the screen is the focusing error. The focus-detection system is assumed to position the lens so that at all magnifications the mask is in exact focus on the film reflective surface. The resulting position of the lens as measured from the film surface is given by*

$$q' = K' \frac{1 - \sqrt{1 - 4f'/K'}}{2} \qquad \text{(A-1)}$$

where f' is the focal length of the lens for the spectral band of light used for the focus-detection system, (f is the visual focal length of the lens). The position of the mask is given by K', which is the distance from the film surface to the mask. Reference to Fig. I-18 will aid in visualizing these distances. The distance from the lens to the screen is now

$$L - q' = p \qquad \text{(A-2)}$$

where L is the distance from film surface to screen. The in-focus point for the visual screen is given by

$$q = \frac{pf}{p - f} \qquad \text{(A-3)}$$

where q is measured from the lens. The error in focus is then

$$E = q' + t - q \qquad \text{(A-4)}$$

*This formula is obtained by solution of the lens formula under the constraint that the distance between image and object is fixed at K'.

where t is the film thickness.

$$E = q' + t - \frac{L - q'}{\frac{L - q'}{f} - 1} \tag{A-5}$$

$$= \frac{\frac{L - q'}{f}(q' + t) - q' - t - L + q'}{\frac{L - q'}{f} - 1}$$

$$E = \frac{(q' + t)(L - q') - f(L + t)}{L - q' - f} \tag{A-6}$$

where

$$q' = K' \frac{1 - \sqrt{1 - 4\frac{f'}{K'}}}{2} \quad .$$

Normalizing,

$$E_n = \frac{E}{L} = \frac{(q_n' + t_n)(1 - q_n') - (1 + t_n) f_n}{1 - q_n' - f_n} \tag{A-7}$$

where

$$q_n = \frac{\gamma}{2}\left(1 - \sqrt{1 - 4\frac{k}{\gamma} f_n}\right) \quad , \tag{A-8}$$

and

$$f_n = \frac{f}{L} \quad , \quad \gamma = \frac{K'}{L} \quad , \quad t_n = \frac{t}{L} \quad k = \frac{f'}{f} \quad .$$

To check, let $\gamma = k = 1$; then

$$q_n' = \frac{1}{2} - \frac{1}{2}\sqrt{1 - 4f_n} \tag{A-9}$$

and

$$1 - q_n' = \frac{1}{2} + \frac{1}{2}\sqrt{1 - 4f_n} \quad ; \tag{A-10}$$

then

$$q_n\,(1 - q_n') = \frac{1}{4} - \frac{1}{4}\,(1 - 4f_n) = f_n \quad . \tag{A-11}$$

Substituting Eqs. (A-9), (A-10), and (A-11) into Eq. (A-7):

$$E_n = \frac{f_n + \frac{t_n}{2}\,(1 + \sqrt{1 - 4f_n}) - f_n - t_n f_n}{\frac{1}{2} + \frac{1}{2}\sqrt{1 - 4f_n} - f_n} \tag{A-12}$$

$$= \frac{\frac{t_n}{2}\,(1 + \sqrt{1 - 4f_n}) - t_n f_n}{\frac{1}{2}\,(1 + \sqrt{1 - 4f_n}) - f_n}$$

$$= t_n \frac{\frac{1}{2}\,(1 + \sqrt{1 - 4f_n}) - f_n}{\frac{1}{2}\,(1 + \sqrt{1 - 4f_n}) - f_n}$$

$$E_n = t_n \quad . \tag{A-13}$$

Thus in the case where visual focal length and detection-system focal length are the same (a perfect achromatic lens), and the mask and screen are exactly the same distance from the film, the focusing error is constant and equal to the film thickness.

For purposes of discussion, it is useful to define a quantity m^* such that

$$\frac{(m^* + 1)^2}{m^*} = f_n \quad . \tag{A-14}$$

This quantity is very close to the actual magnification at which the system is operating.

APPENDIX B

CONVOLUTION OF CIRCLES OF DIFFERENT DIAMETERS

APPENDIX B

CONVOLUTION OF CIRCLES OF DIFFERENT DIAMETERS

We are interested here in deriving the common area A between two circles having different radii r and R as their relative separation S is varied (see Fig. B-1). The method of approach is to set up a double

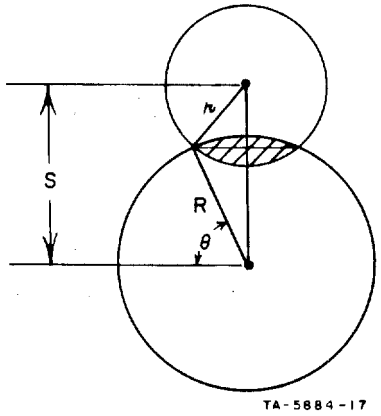

FIG. B-1 ARRANGEMENT FOR COMPUTING COMMON AREA BETWEEN TWO UNEQUAL OVERLAPPING DISKS

integration in order to calculate the cross-hatched common area:

$$A = 2 \int_0^{R\cos\theta} dx \int_{S-\sqrt{r^2-x^2}}^{\sqrt{R^2-x^2}} dy \qquad \text{(B-1)}$$

where θ is the angle shown in Fig. B-1. The relation between θ and S is derived from

$$S = r \sin \alpha + R \sin \theta \qquad \text{(B-2)}$$

and

$$R \cos \theta = r \cos \alpha \quad . \tag{B-3}$$

Substituting Eq. (B-3) into Eq. (B-2) we find

$$S = r \sqrt{1 - \left(\frac{R}{r}\right)^2 \cos^2 \theta} + R \sqrt{1 - \cos^2 \theta} \tag{B-4}$$

which can be manipulated to the form

$$\cos^2 \theta = 1 - \left[\frac{S^2 + R^2 - r^2}{2SR}\right]^2 \quad . \tag{B-5}$$

Let us continue with the evaluation of Eq. (B-1) and then substitute the value of cos θ from Eq. (B-5). The indefinite integral of the function $\sqrt{a^2 - x^2}$ is

$$\int \sqrt{a^2 - x^2}\, dx = \frac{1}{2}\left[x \sqrt{a^2 - x^2} + a^2 \sin^{-1}\left(\frac{x}{a}\right)\right] \quad . \tag{B-6}$$

Applying Eq. (B-5) to Eq. (B-1), we obtain

$$A = R^2 \cos \theta \left[\sqrt{1 - \cos^2\theta} + \sqrt{\left(\frac{r}{R}\right)^2 - \cos^2\theta} - \frac{2S}{R}\right] + R^2 \sin^{-1} (\cos \theta)$$

$$+ r^2 \sin^{-1}\left(\frac{R \cos \theta}{r}\right) \tag{B-7}$$

which can be converted by means of Eq. (B-5) to the form

$$A = - RS \cos \theta + R^2 \sin^{-1} (\cos \theta) + r^2 \sin^{-1}\left(\frac{R \cos \theta}{r}\right) \quad . \tag{B-8}$$

To check the validity of Eq. (B-8), we note that for r = R and S = 0, Eq. (B-5) correctly predicts that cos θ = 1 (or θ = 0), and Eq. (B-8) correctly predicts $A = \pi R^2$. Also, for r = R, and S = 2R (i.e.,

externally tangent circles), Eq. (B-5) correctly predicts cos $\theta = 0$ (or $\theta = \pi/2$) and Eq. (B-8) correctly predicts $A = 0$.

Now we must note that Eq. (B-6) applies only for $S \geq S_c$ where $S_c = \sqrt{R^2 - r^2}$. How this limitation comes about can be seen from Fig. B-2(a). When $S = S_c$, the center of the smaller circle lies exactly on the common chord of intersection. This case represents the largest

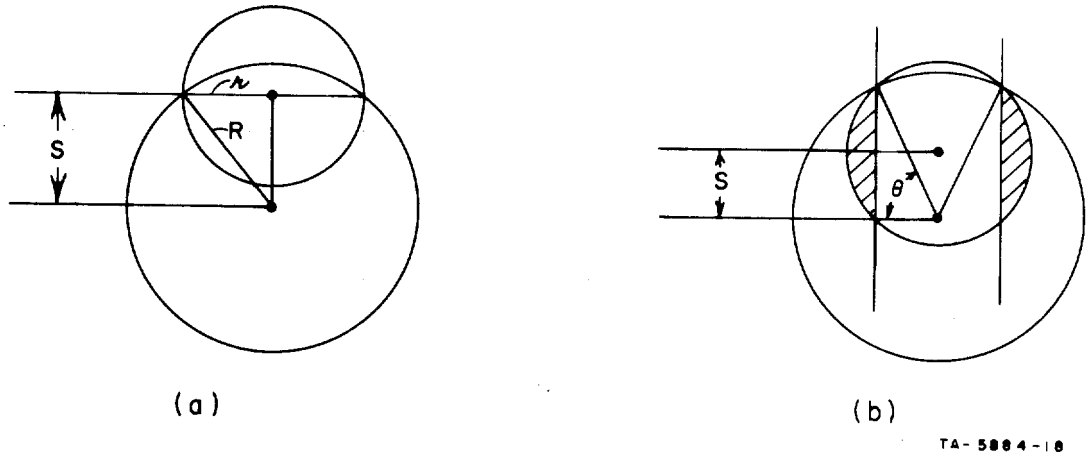

FIG. B-2 COMPUTATION OF OVERLAP AREA FOR SMALL VALUES OF SEPARATION

possible chord of intersection, namely the diameter of the smaller circle. For $S < S_c$, the integral in Eq. (B-1) is incomplete since it accounts only for the area bounded by the heavy lines in Fig. B-2(b), but not the cross-hatched areas. The area A' of the cross-hatched regions is readily evaluated from

$$A' = 4 \int_{R\cos\theta}^{r} \sqrt{r^2 - x^2}\, dx \qquad \text{(B-9)}$$

which by application of Eq. (B-6) reduces to

$$A' = \pi r^2 - 2R^2 \cos\theta \left[\sqrt{\left(\frac{r}{R}\right)^2 - \cos^2\theta}\right] - 2r^2 \sin^{-1}\left(\frac{R\cos\theta}{r}\right) . \qquad \text{(B-10)}$$

Adding A' to Eq. (B-8) and simplifying, we obtain for $0 \leq S \leq \sqrt{R^2 - r^2}$

$$A = \pi r^2 - R \cos\theta \left(\frac{R^2 - r^2 - 2S^2}{S}\right) + R^2 \sin^{-1}(\cos\theta) - r^2 \sin^{-1}\left(\frac{R\cos\theta}{r}\right) \quad . \qquad \text{(B-11)}$$

To verify these relations note that for $S = \sqrt{R^2 - r^2}$ Eq. (B-5) correctly predicts $\cos\theta = r/R$, and Eqs. (B-7) and (B-11) predict the identical value of area, namely

$$A = \frac{\pi r^2}{2} - r\sqrt{R^2 - r^2} + R^2 \sin^{-1}\left(\frac{r}{R}\right) \qquad \text{(B-12)}$$

which predicts the correct value of A as $R \to \infty$, since the common arc through the smaller circle then becomes a straight line, and we expect simply that $A \to \pi r^2/2$.

Figure B-3 shows a set of computer results for various ratios of R/r. Note that for R/r = 20 the curve is almost symmetric, as it should be for $R/r \to \infty$. For R = r, the curve is remarkably linear. The curve shape changes rapidly with small increases in R/r, the R/r = 2 curve lying almost halfway between the R/r = 1 and R/r = 20 curves.

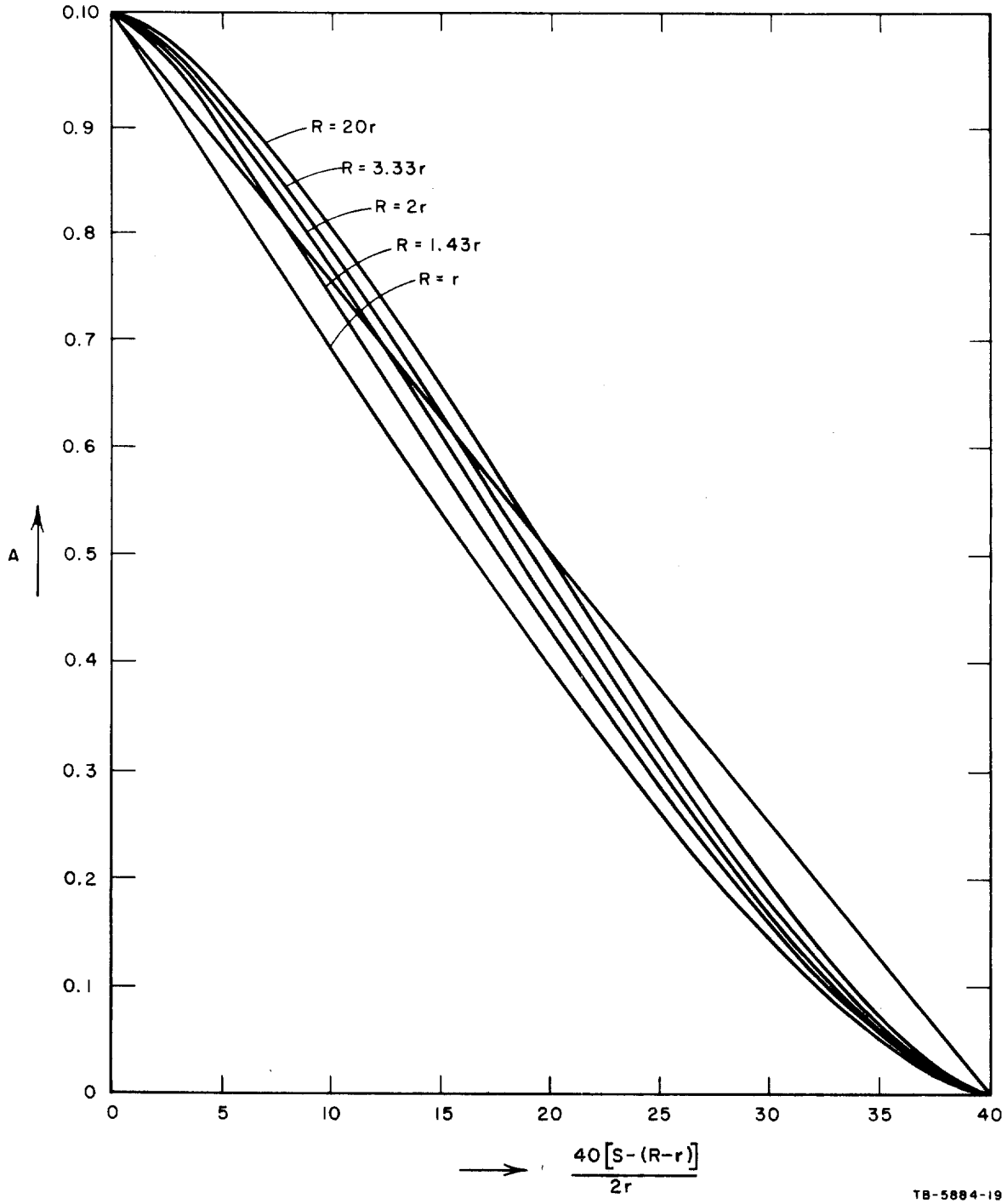

FIG. B-3 COMPUTER-GENERATED CURVES OF COMMON AREA AS A FUNCTION OF SEPARATION S OVER THE RANGE $R-r \leq S \leq R+r$ FOR DIFFERENT RADIUS RATIOS

APPENDIX C

PROOF OF NO TRUNCATION LOSS IN RANGE $0 \leq \Delta p \leq \Delta p_c^+$

APPENDIX C

PROOF OF NO TRUNCATION LOSS IN RANGE $0 \leq \Delta p \leq \Delta p_c^+$

Our goal here is to prove that over the range $0 \leq \Delta p_c \leq \Delta p_c^+$ the truncation by the lens of the reimaging cone does not have to be considered in calculating intercepted light.

Referring back to Fig. II-11, assume first that the lens does not truncate the reimaging cone at r'', and that a pure disk of diameter W' is intercepted in the object plane, with the center of the disk displaced S' from the optical axis. Let us immediately jump to consideration of the $\Delta p = \Delta p_c^+$ condition, in which case $W' = W$ (that is, the intercepted disk is exactly the same size as the object disk). Substituting Eq. (II-32) for $\Delta p_c^+/p$ into Eq. (II-50) for S' we obtain

$$S' = r\,(1 - \alpha) \tag{C-1}$$

which for the largest value of r, namely $r = W/2$, becomes

$$S' = \frac{W}{2}\,(1 - \alpha) \quad . \tag{C-2}$$

Before we can use these relations for W' and S' we must return to the lens plane and determine the form of the truncated cone formed by lens blockage, in particular the width z of the truncated zone in Fig. II-12(a).

From Eq. (II-33), we see that in terms of mirror position

$$\frac{\Delta q_{Mc}^-}{q} = -\frac{\alpha}{2} \quad . \tag{C-3}$$

Substituting Eq. (II-33) into Eqs. (II-13) and (II-14), we have

$$D' = D\,(1 - \alpha) \quad , \tag{C-4}$$

$$S = \frac{D}{2} \alpha (2 - \alpha) \quad . \tag{C-5}$$

Now the truncation distance z is simply

$$z = (S + R') - R = \frac{D}{2} \alpha (1 - \alpha) \quad . \tag{C-6}$$

The fraction of the radius of disk R' that is truncated is

$$\frac{z}{R'} = \frac{\frac{D}{2} \alpha (1 - \alpha)}{\frac{D}{2} (1 - \alpha)} = \alpha \quad . \tag{C-7}$$

With this result, we can now return to the object plane and complete our proof.

The same truncation fraction z clearly applies in the object plane, so that in Fig. II-12(c) we have

$$z' = \frac{W}{2} (\alpha) \quad . \tag{C-8}$$

What we wish to show now is that the truncating arc, which is part of a larger (dashed) circle of diameter W/2 (1/1 - α) falls exactly on the intersection point of the two equal-area circles of diameter W. To demonstrate this we consider the darkened triangle and show that the value x (which is the distance from the center of the larger circle to the intersection point) is just equal to the diameter of the larger circle, so that the large circle does in fact pass through the intersection point.

To solve for x, we must find y and θ. One point that we can note immediately is that the truncation arc passes exactly through the center of the lower circle, since the truncation distance $z' = W/2\ \alpha$ exactly compensates for the amount by which the separation S' [Eq. (C-2)] is short of a complete radius of separation; this amount is $W/2\ \alpha$. With this simple observation, we can write

$$y = \frac{W'}{2} - S \qquad \text{(C-9)}$$

where $W'/2$ is the radius of the larger circle, or

$$y = \frac{W}{2}\left(\frac{1}{1-\alpha}\right) - \frac{W}{2}(1-\alpha) = \frac{W}{2}\left(\frac{2-\alpha}{1-\alpha}\right)\alpha \quad . \qquad \text{(C-10)}$$

Now the value x can be written as

$$x^2 = y^2 + \left(\frac{W}{2}\right)^2 - 2y\left(\frac{W}{2}\right)\cos\left(\frac{\pi}{2} + \theta\right) \quad . \qquad \text{(C-11)}$$

We find from Eq. (B-5) of Appendix B that

$$\cos^2\theta = 1 - \left[\frac{S^2 + R^2 - r^2}{2SR}\right]^2 \quad . \qquad \text{(B-5)}$$

where R and r are the general radii of the two intersecting circles. In our case, the circles have equal radii, namely $R = r = W/2$. Furthermore, we are really interested in sin θ, since cos $[(\pi/2) + \theta] = -\sin\theta$, and we can write

$$\sin^2\theta = 1 - \cos^2\theta = \left(\frac{S}{2R}\right)^2 \quad . \qquad \text{(C-12)}$$

But in our case $S = S' = W/2\ (1-\alpha)$, and $R = W/2$, so that

$$\sin\theta = \frac{1-\alpha}{2} \quad . \qquad \text{(C-13)}$$

Substituting into Eq. (C-11) we find

$$x^2 = \left(\frac{W}{2}\right)^2\left[\left(\frac{2-\alpha}{1-\alpha}\right)^2\alpha^2 + 1 + 2\left(\frac{2-\alpha}{1-\alpha}\right)\alpha\left(\frac{1-\alpha}{2}\right)\right] \qquad \text{(C-14)}$$

from which we have

$$x = \frac{W/2}{1-\alpha} \qquad \text{(C-15)}$$

which is precisely what we wished to show.

What we have in effect shown is that for $\Delta p = \Delta p_c^+$ the truncation portion of the converging cone would have passed completely back through the object aperture anyway, and so does not affect the calculation of intercepted light. We have shown this for the extreme value $r = W/2$. If it is true for $r = W/2$, it is clearly true for smaller values of r, so the conclusion is true for every point on the disk. Furthermore, if the conclusion is true for $\Delta p = \Delta p_c^+$ it is also clearly true for all smaller values of Δp over the range $0 \leq \Delta p \leq \Delta p_c^+$.

APPENDIX D

PROOF OF NO TRUNCATION LOSS IN THE RANGE $0 \leq \Delta p \leq \Delta p_c^-$

APPENDIX D

PROOF OF NO TRUNCATION LOSS IN THE RANGE $0 \leq \Delta p \leq \Delta p_c^-$

In Appendix C we showed that over the range $0 \leq \Delta p \leq \Delta p_c^+$, any return light that does not pass the lens will have passed through the object aperture anyway, and therefore need not be accounted for in computing the intercepted light L_I.

Interestingly, a similar conclusion can be drawn for the range $0 \leq \Delta p \leq \Delta p_c^-$ if we properly define the "truncated" returning disk of light. However, there is an important new intensity effect that must be included in the integration for intercepted light L_I.

In the derivation of Appendix C, for the range $0 \leq \Delta p \leq \Delta p_c^+$, the return disk of light in the lens plane is smaller than the lens in diameter and has a portion truncated by the lens [Fig. 12(a)]. For the range $0 \leq \Delta p \leq \Delta p_c^-$ the return disk in the lens plane is larger than the lens, and it turns out to be more convenient in this case to view the returning light that passes the lens (cross-hatched region in Fig. D-1) as deriving from the lens disk itself, but with a small truncated segment of height z. (Actually, it is not a truncation in the earlier sense; rather there is no light in this region.)

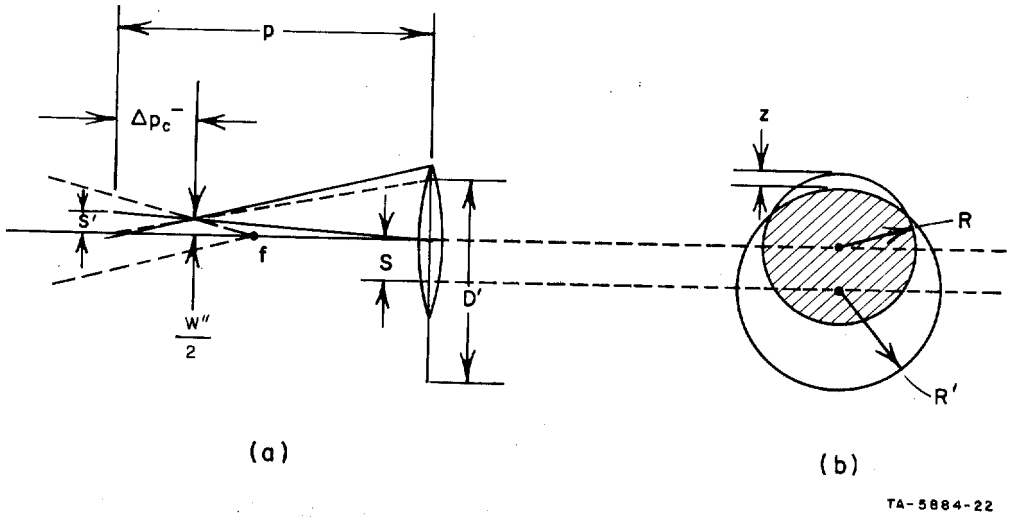

FIG. D-1 GEOMETRIC CONFIGURATION FOR $\Delta p = \Delta p_c^-$

Note that for an object point above the axis [Fig. D-1(a)], there is a downward displacement S of the returning disk, and the truncated portion occurs at the top of the lens disk. The truncated cone comes to focus in the Δp_c^- plane and then spreads out again so that in the object plane the truncated portion now appears at the bottom of the disk. What we would like to show is that at the extreme of the range, namely $\Delta p = \Delta p_c^-$, exactly the same condition holds as in Fig. II-12(c).

From Eqs. (II-39) and (II-40) we see that

$$\frac{\Delta p_c^-}{p} = - \frac{W}{D + W} \tag{D-1}$$

and in terms of Δq

$$\frac{\Delta q_c^+}{q} = \frac{\alpha}{1 - \alpha} \quad . \tag{D-2}$$

For this condition, we have the following expressions for D' and S, from Eqs. (II-13) and (II-14):

$$D' = D \left(1 + \frac{\Delta q_c^+}{q}\right) = D \frac{1}{1 - \alpha} \quad , \tag{D-3}$$

$$S = \frac{Wq}{p} \left(1 + \frac{1}{2} \frac{\Delta q_c^+}{q}\right) = \frac{D}{2} \alpha \frac{2 - \alpha}{1 - \alpha} \quad . \tag{D-4}$$

We readily compute the truncation distance z as

$$z = R - (R' - S) = \frac{D}{2} \alpha \tag{D-5}$$

or, as a fraction of the radius of the circle being truncated (namely the lens disk) we have, in analogy to Eq. (C-7),

$$\frac{z}{R} = \alpha \quad . \tag{D-6}$$

Now by the definition of Δp_c^- we know that the diameter of the blur disk in the object plane is equal to that of the disk object itself,

namely W. We have then just one other quantity to determine, namely the displacement S' of the truncated blur disk in the object plane.

From Fig. D-1(a) we have the geometric relation

$$\frac{S'}{p} = \frac{W''/2}{p + \Delta p_c^-} \qquad \text{(D-7)}$$

where W'' is the diameter of the in-focus disk in the Δp_c^- plane, which from Eq. (II-6) takes the form

$$\frac{W''}{2} = \frac{W}{2} \frac{p + \Delta p - f}{p - f} \qquad \text{(D-8)}$$

$$S' = \frac{W}{2} \frac{p + \Delta p_c^- - f}{p - f} \frac{p}{p + \Delta p_c^-} \qquad \text{(D-9)}$$

which by substitution of Eq. (D-1) reduces to

$$S' = \frac{W}{2} (1 - \alpha) \quad . \qquad \text{(D-10)}$$

But these are exactly the same conditions as in the proof of Appendix C, namely two equal circles (our circles of diameter W), displaced by a distance $S' = W/2\ (1 - \alpha)$, with a truncation fraction α that derives from a pair of circles whose diametric ratio is $(1 - \alpha)$; i.e., our lens-plane circles D and D'.

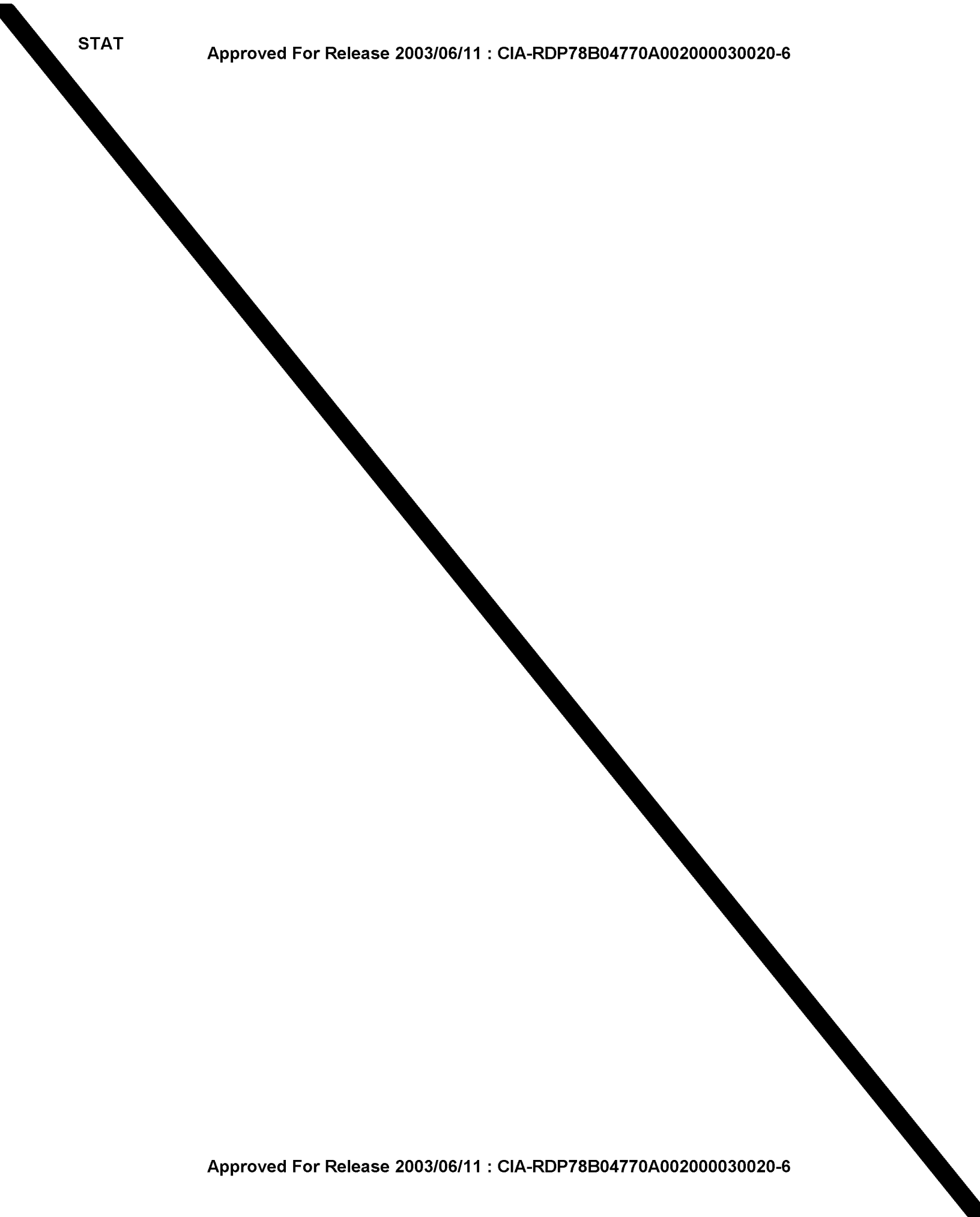

Approved For Release 2003/06/11 : CIA-RDP78B04770A002000030020-6